Politecnico di Torino

Abstract of Master Thesis in Mechanical Engineering:

"MATLAB FE-code writing for a 3D-simulation and dynamic analysis of multi-span ropeway system"

Supervisor:

Prof. Luigi Garibaldi

Student:

Mojtaba Ahani

Date:

September 2021

1 Contents

2 Introduction

2.1 Cable transport systems and State of art

Cable Transport is a wide means of transportation characterized by one or more cables. They often utilize vehicles called cable cars to transport passengers and goods while the cable may be of different types driven or passive. A cable car (U.K., Europe), similarly called an aerial lift (U.S.), is one type of cable transport mechanism that hauls cabins, cars, gondolas, or open chairs above the ground through several cables. Aerial lift systems have been extensively adopted in places where building roads are not convenient such as mountainous territories and even mining sites. Unfortunately, despite maximum care, which is being taken within their missions, there are still accidents happening every year. Although some of them are due to human mistakes, yet a great deal of them occurs owing to a combination of poor engineering design and operational conditions.

A gondola lift is a type of cable car which is made up of only one wire rope generally of steel material. The cable is circulated and strung between two stations and usually passing over multiple intermediate-supporting towers. An engine or electric motor is utilized to drive the cable with a constant line speed through a bull wheel in a terminal to provide propulsion within the operation.

Figure 2.1 _ Gondola lift

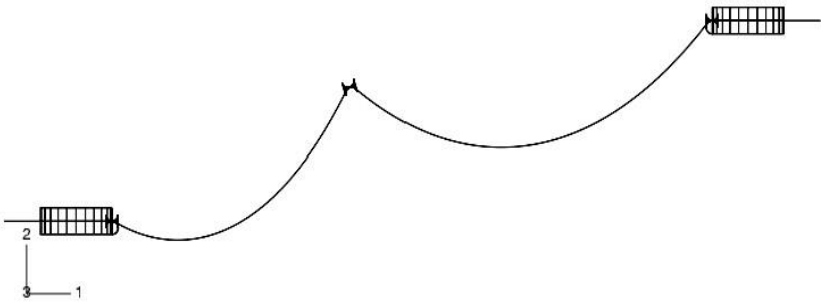

Figure 2.2 _ An illustrative 3D model of a gondola lift with two spans

Another kind of cable car is a ropeway (even known as an aerial tramway, sky tram, or aerial tram), characterized by using one or two stationary ropes (track cables) as supports for passenger or cargo cabins. These cabins are rigidly connected to a set of wheels named the truck rolling on the track cables. Additionally, another moving rope is implemented so that provides propulsion (haulage rope). Within this type of system, an aerial tramway cabin's grip is fixed onto the haulage rope that is driven by an electric motor throughout the operation.

Figure 2.3 _ Aerial Tramway

In a gondola lift, moving cable carries loads and masses fixed to the cable itself and according to previous work, we can analyze it as a fixed cable subjected to moving loads and masses with minor and negligible error. Speaking of ropeways, ignoring the interaction of moving rope on the track cable (stationary one), which is a negligible effect, we can adopt the same consideration to study the behavior of the track cable. In conclusion, our simulation holds for the two system configurations.

The cable in gondola lifts and the track cables in ropeways are subjected to various loading conditions in both vertical (parallel to the field of gravity) and lateral direction (orthogonal to the field of gravity) such as the weight of multiple moving mass in the vertical and wind in the lateral direction. Each one of these loadings may contribute to severe conditions that eventually end up in strand fatigue failure usually taking place at points where the cable motion is constrained against transverse vibration, such as at suspensions and boundaries. As a result, it is necessary to analyze the dynamic behavior of the system under these

situations. Owing to difficulties in operating measurements on the field, studying the system dynamic response mostly relies on numerical analysis.

Since there are not many published works in this regard, this work is dedicated to deal with the above issues and address the challenges we face when simulating the track cable. The main objective that concerns this work is initially developing FE-code in MATLAB to perform a three-dimensional simulation of a multi-span beam as a (track) cable having each span with different lengths and orientations in space. In this case, the system has been discretized by adopting a 1D Euler-Bernoulli beam element. Euler-Bernoulli beam element has two nodes on which the inertia, damping, and stiffness properties are lumped, and six degrees of freedom are associated with each node. Afterward, having a global mass matrix and global stiffness matrix of the entire structure, modal analysis of the system was carried out to extract the mode shapes associated with the first five smallest natural frequencies of the system which can be considered as the most important ones among the others.

2.2 Work organization

Validation of the developed MATLAB model is an essential step to proceed with this project's remaining tasks, which mainly involves analysis of the dynamic behavior of the system. Consequently, validation has been carried out firstly by using commercial FEM software (ABAQUS) to perform modal analysis. Within ABAQUS simulation, the B33 element type was adopted which represents quadratic E-B beam element in space. Subsequently, further assessment of the MATLAB FE-model accomplished through successfully generating the correct results and mode shapes for a multi-span Euler-Bernoulli beam carrying several various concentrated elements including point masses, rotary inertias, linear springs, rotational springs, and spring-mass systems. This system is investigated in a paper.

To study the dynamic behavior of the system, initially, as the real system is subjected to various loadings, it is necessary to analyze a different kind of forced responses of the system. Accordingly, step response, harmonic response, and the response of the system to multiple moving loads and even multiple moving masses have been investigated in the current work, in which the latter represents several cargo cabins passing through the (track) cable in the vertical plane. On the other side, wind pressure over the moving cabins has been studied which simply means excitation in the lateral plane. In order to perform these analyses, the Newmark algorithm has been adopted in this work, which is an implicit time integration scheme to discretize second-order time systems and widely used for structural dynamic analysis.

2.3 Literature review

3 Modelling and Simulation approach

The finite element method has been utilized in this work which either is one of the most widely adopted techniques to discretize systems. The possibility of using this approach for a vast variety of problems and more importantly the increasing power of computing machines available, has made this method reliable and more successful. Usually, the systems modeled using this method end up with a large number (hundreds, thousands, or even millions) of degrees of freedom, although the obtained ODEs can be easily implemented in both time-domain and frequency-domain computations.

3.1 Introduction to the adopted Finite element approach and formulation

3.1.1 Euler-Bernoulli element and formulation (G.Genta, 2008)

Among different approaches in finite element, the beam element is one of the most frequently adopted elements and is available in all software and computer codes. There are numbers of beam formulations developed which differ based on the number of nodes and degrees of freedom on each element and the theoretical formulation.

Euler-Bernoulli element is a prismatic homogeneous beam that does not consider the shear deformation and has been utilized in this work. In 3D configuration, the element includes one node of six DOFs at each end and, three translational displacements, and three rotations ending up with 12 DOFs per element. The nodal displacement vector will be:

$$\{q\} = \{u_{z1}\ u_{x1}\ u_{y1}\ \theta_{z1}\ \theta_{x1}\ \theta_{y1}\ u_{z2}\ u_{x2}\ u_{y2}\ \theta_{z2}\ \theta_{x2}\ \theta_{y2}\}'_{1\times12}$$

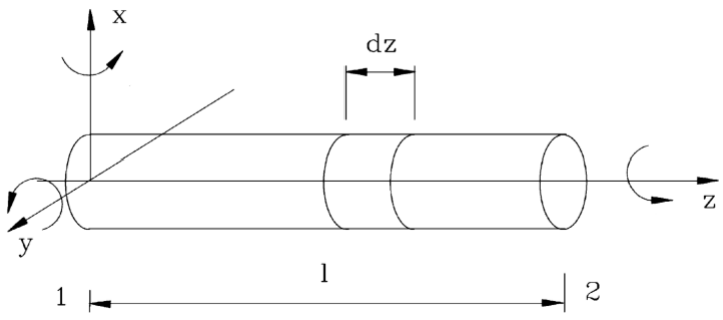

Figure 3.1 _ Beam element and reference frame

Axial behavior – z direction

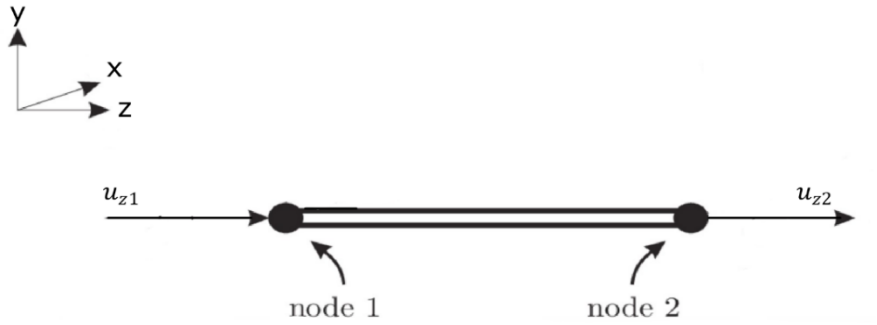

Figure 3.2 _ Euler-Bernoulli beam element and axial degrees of freedom

In this case, the beam can be conceived as a bar, and there is only one degree of freedom at each point which is axial translational displacement along the z axis (u_z), the nodal displacement vector q_A has two rows and one column. Either the shape function matrix N_A corresponding to the axial behavior is a matrix of one row and two columns (there are only two DOFs in the element).

$$\mathbf{\{q_A\}} = \begin{Bmatrix} u_{z1} \\ u_{z2} \end{Bmatrix} \qquad \mathbf{N_A} = [1 - \zeta \quad \zeta]$$

Which $\zeta = z/l$, and l is the length of element.

The matrices of the element in the axial behavior would be as the following:

$$\mathbf{K}_A = \frac{EA}{l} \begin{bmatrix} 1 & -1 \\ -1 & 1 \end{bmatrix}$$

$$\mathbf{M}_A = \frac{\rho A l}{6} \begin{bmatrix} 2 & 1 \\ 1 & 2 \end{bmatrix}$$

Torsional behavior

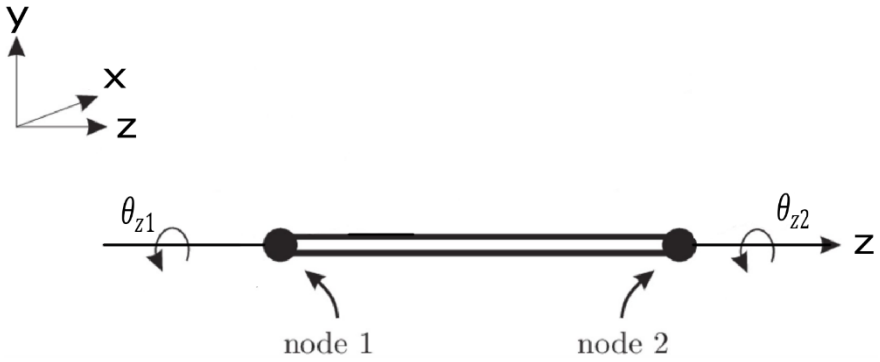

Figure 3.3 _ Euler-Bernoulli beam element and torsional degrees of freedom

As what has been discussed in axial behavior, the equation of motion concerning the torsional behavior of the Euler-Bernoulli element is identical to those of axial behavior; except for the fact that the degrees of freedom, in this case, is rotation in z axis (θ_z). The shape function matrix N_T and the nodal displacement vector q_T are either of the same dimension:

$$\{q_T\} = \begin{Bmatrix} \theta_{z1} \\ \theta_{z2} \end{Bmatrix} \qquad N_T = [1 - \zeta \quad \zeta]$$

Which $\zeta = z/l$, and l is the length of element.

And the expression of the matrices is:

$$K_T = \frac{GI'_p l}{l} \begin{bmatrix} 1 & -1 \\ -1 & 1 \end{bmatrix}$$

$$M_T = \frac{\rho I_p l}{6} \begin{bmatrix} 2 & 1 \\ 1 & 2 \end{bmatrix}$$

Flexural behavior – xz plane

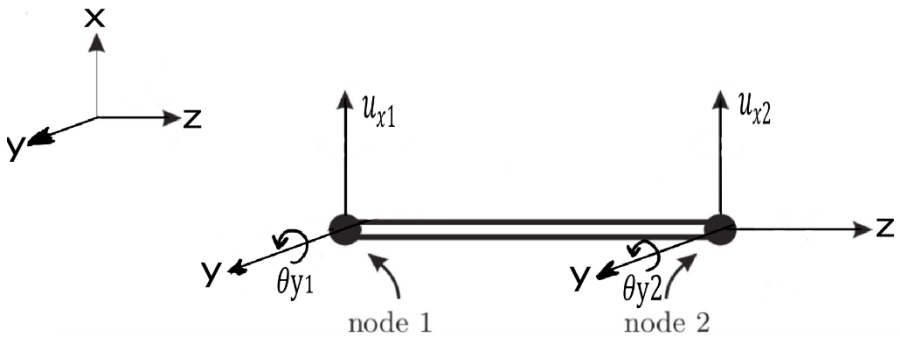

Figure 3.4 _ Euler-Bernoulli beam element and flexural degrees of freedom within xz plane

To each node are associated two DoFs, a translational one along the x axis (u_x) and a rotational one around the y axis (θ_y). This means that the mass, stiffness, and damping matrices associated to this discretized element have a 4×4 size.

in this case, the shape function matrix N_{F1} and the nodal displacement vector q_{F1} are as the following:

$$\mathbf{\{q_{F1}\}} = \{u_{x1} \;\; \theta_{y1} \;\; u_{x2} \;\; \theta_{y2}\}'_{1\times4} \qquad \mathbf{N_{F1}} = \begin{bmatrix} N_{11} & N_{12} & N_{13} & N_{14} \\ N_{21} & N_{22} & N_{23} & N_{24} \end{bmatrix}$$

Which:

$$N_{11} = 1 - 3\zeta^2 + 2\zeta^3 \qquad N_{21} = \frac{6\zeta}{l}(\zeta - 1)$$

$$N_{12} = l\zeta(1 - 2\zeta + \zeta^2) \qquad N_{22} = (1 - 4\zeta + 3\zeta^2)$$

$$N_{13} = \zeta(3\zeta - 2\zeta^2) \qquad N_{21} = \frac{-6\zeta}{l}(\zeta - 1)$$

$$N_{14} = l\zeta(-\zeta + \zeta^2) \qquad N_{24} = -2\zeta + 3\zeta^2)$$

For each element the stiffness matrix is:

$$\boldsymbol{K_{xz}} = \frac{EI}{L^3}\begin{bmatrix} 12 & 6L & -12 & 6L \\ 6L & 4L^2 & -6L & 2L^2 \\ -12 & -6L & 12 & -6L \\ 6L & 2L^2 & -6L & 4L^2 \end{bmatrix}$$

While the mass matrix, since we adopted a consistent mass matrix approach, is given by:

$$\boldsymbol{M}_{xz} = \frac{\rho AL}{420}\begin{bmatrix} m_1 & Lm_2 & m_3 & -Lm_4 \\ Lm_2 & L^2m_5 & Lm_4 & -L^2m_6 \\ m_3 & Lm_4 & m_1 & -Lm_2 \\ -Lm_4 & -L^2m_6 & -Lm_2 & L^2m_5 \end{bmatrix} + \frac{\rho I_y}{30\mathrm{L}}\begin{bmatrix} m_7 & Lm\text{-}_8 & -m_7 & Lm_8 \\ Lm_8 & L^2m_9 & -Lm_8 & L^2m_{10} \\ -m_7 & -Lm_8 & m_7 & -Lm_8 \\ Lm_8 & L^2m_{10} & -Lm_8 & L^2m_9 \end{bmatrix}$$

Where the coefficients of the mass matrix are obtained substituting the expression of the shape function into kinetic energy and integrating it the m values for Euler-Bernoulli beam.

The mass coefficient expressions are:

$$m_1 = 156 \qquad m_6 = 3$$
$$m_2 = 22 \qquad m_7 = 36$$
$$m_3 = 54 \qquad m_8 = 3$$
$$m_4 = 13 \qquad m_9 = 4$$
$$m_5 = 4 \qquad m_{10} = 1$$

The load vector due to distributed shear force $f_x(t)$ and bending moment $m_y(t)$ would be:

$$\mathbf{f}(t)_{F1} = \frac{l f_x(t)}{12}\begin{Bmatrix} 6 \\ l \\ 6 \\ -l \end{Bmatrix} + m_y(t)\begin{Bmatrix} -l \\ 0 \\ l \\ 0 \end{Bmatrix}$$

Flexural behavior – yz plane

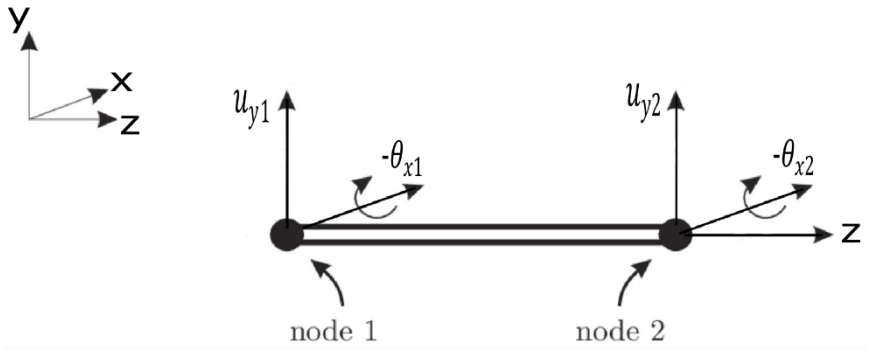

Figure 3.5 _ Euler-Bernoulli beam element and flexural degrees of freedom within yz plane

In this case, as what has been discussed about flexural behavior in the xz-plane, to each node are associated two DoFs a translational one along the y axis (u_y) and a rotational one around the x axis (θ_x). This means that the mass, stiffness, and damping matrices associated with this discretized element have a 4×4 size. Due to different signs of rotations, we need to use equations different from those in the xz-plane.

The matrices, in this case, could easily be obtained from those achieved for xz-plane by a simple change of signs of elements with subscripts 12, 14, 21, and 23 in shape function matrix N_{F1} and either the elements with subscripts 12, 14, 23, and 34 and their symmetrical ones in mass and stiffness matrices. With respect

to external force vector, and external moments, we only need to change the signs of elements 2 and 4 or 1 and 3.

$\mathbf{\{q_{F2}\}} = \{u_{y1} \;\; \theta_{x1} \;\; u_{y2} \;\; \theta_{x2}\}'_{1\times4}$ $\qquad\qquad$ $\mathbf{N_{F2}} = \begin{bmatrix} N_{11} & -N_{12} & N_{13} & -N_{14} \\ -N_{21} & N_{22} & -N_{23} & N_{24} \end{bmatrix}$

For each element the stiffness matrix is:

$$\boldsymbol{K}_{yz} = \frac{EI}{L^3}\begin{bmatrix} 12 & -6L & -12 & -6L \\ -6L & 4L^2 & 6L & 2L^2 \\ -12 & 6L & 12 & 6L \\ -6L & 2L^2 & 6L & 4L^2 \end{bmatrix}$$

While the mass matrix, since we adopted a consistent mass matrix approach, is given by:

$$\boldsymbol{M}_{yz} = \frac{\rho AL}{420}\begin{bmatrix} m_1 & -Lm_2 & m_3 & Lm_4 \\ -Lm_2 & L^2m_5 & -Lm_4 & -L^2m_6 \\ m_3 & -Lm_4 & m_1 & Lm_2 \\ Lm_4 & -L^2m_6 & Lm_2 & L^2m_5 \end{bmatrix} + \frac{\rho I_x}{30\mathrm{L}}\begin{bmatrix} m_7 & -Lm\text{-}_8 & -m_7 & -Lm_8 \\ -Lm_8 & L^2m_9 & Lm_8 & L^2m_{10} \\ -m_7 & Lm_8 & m_7 & Lm_8 \\ -Lm_8 & L^2m_{10} & Lm_8 & L^2m_9 \end{bmatrix}$$

The load vector due to distributed shear force $f_y(t)$ and bending moment $m_x(t)$ would be:

$$\mathbf{f}(\mathrm{t})_{\mathrm{F2}} = \frac{lf_y(t)}{12}\begin{Bmatrix} 6 \\ -l \\ 6 \\ l \end{Bmatrix} + m_x(t)\begin{Bmatrix} -l \\ 0 \\ l \\ 0 \end{Bmatrix}$$

3.1.2 Effect of axial force on flexural behavior

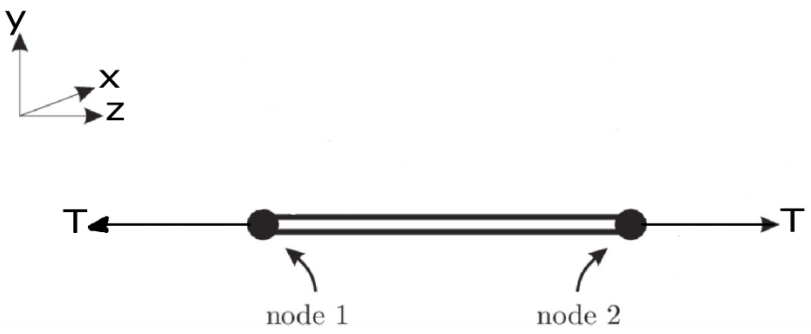

Figure 3.6 _ Euler-Bernoulli beam element with axial force T

The interaction between flexural behavior and axial force in a beam causes geometric nonlinearity. To avoid this nonlinearity, in the case of constant axial load, it is possible to linearize the interaction.

Considering the flexural behavior of the Euler-Bernoulli beam on for example xz-plane, and a constant axial tensile load T is applied on it, it can be simply proven that the tension increases the stiffness. This incremented stiffness can be calculated by the following matrix:

$$\boldsymbol{K_g} = \frac{T}{30l}\begin{bmatrix} k_1 & lk_2 & -k_1 & lk_2 \\ lk_2 & l^2k_3 & -lk_2 & -l^2k_4 \\ -k_1 & -lk_2 & k_1 & -lk_2 \\ lk_2 & -l^2k_4 & -lk_2 & l^2k_3 \end{bmatrix}$$

$$k_1 = 36 \qquad k_2 = 3$$

$$k_3 = 4 \qquad k_4 = 1$$

Simply by adding this matrix to the stiffness of the element, we discussed earlier, the total stiffness of the matrix will be achieved.

3.1.3 Reference frames and rotation matrix

The conventional reference frame for similar systems and what is adopted

So far, we have discussed the beam element with respect to a local right-handed coordinate system so that the z-axis is oriented along the beam axial direction and the field of gravity is toward the negative side of the x-axis. On the contrary, in many pieces of literature and papers, the right-handed coordinate system with x-axis elongated in the axial direction of the beam is more conventional.

Axial behavior – x direction

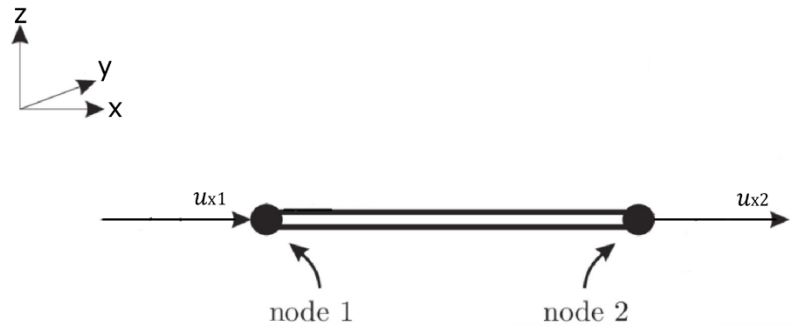

Figure 3.7 _ Euler-Bernoulli beam element and axial degrees of freedom along x direction

In this case, the axial degrees of freedom of the element are as follow:

$$\{\mathbf{q}_A\} = \begin{Bmatrix} u_{x1} \\ u_{x2} \end{Bmatrix}$$

While the other vector and matrices as shape function, stiffness, and mass matrix, and nodal force vector of the element are identical to those we have seen in the previous form of coordinate system concerning axial behavior.

Torsional behavior

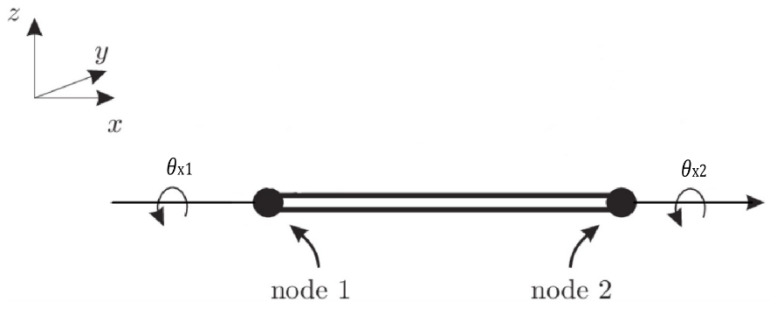

Figure 3.8 _ Euler-Bernoulli beam element and torsional degrees of freedom along x direction

In this case, the torsional degrees of freedom of the element are as follow:

$$\{\mathbf{q_T}\} = \begin{Bmatrix} \theta_{x1} \\ \theta_{x2} \end{Bmatrix}$$

While the other vector and matrices as shape function, stiffness, and mass matrix, and nodal force vector of the element are identical to those we have seen in the previous form of coordinate system concerning torsional behavior.

Flexural behavior – yx plane

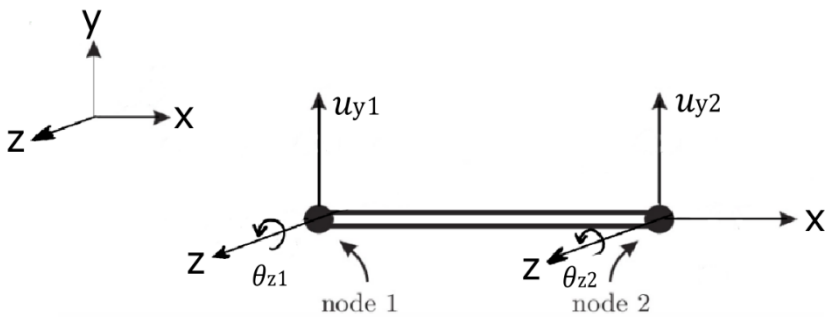

Figure 3.9 _ Euler-Bernoulli beam element and flexural degrees of freedom in yx plane

Degrees of freedom of flexural behavior in yx plane is:

$$\{\mathbf{q}_{F1}\} = \{u_{y1}\ \theta_{z1}\ u_{y2}\ \theta_{z2}\}'_{1\times4}$$

The nodal force vector and shape function, stiffness, and mass matrices are equivalent to those of behavior in xz plane with respect to previous form of coordinate system.

Flexural behavior – zx plane

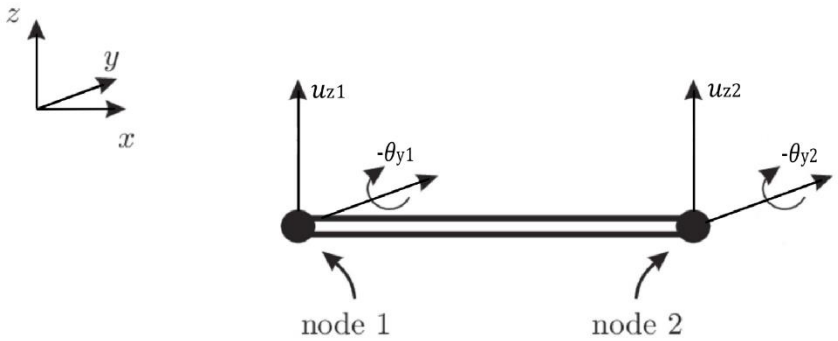

Figure 3.10 _ Euler-Bernoulli beam element and flexural degrees of freedom in zx plane

Degrees of freedom of flexural behavior in zx plane is:

$$\{\mathbf{q}_{\mathrm{F2}}\} = \{u_{z1}\ \theta_{y1}\ u_{z2}\ \theta_{y2}\}'_{1\times4}$$

The nodal force vector and shape function, stiffness, and mass matrices are equivalent to those of behavior in yz plane with respect to previous form of coordinate system.

Following this logic for comparing the different orientations of the coordinate system, the global expression of stiffness and mass matrices with respect to the conventional coordinate system would be identical to what we have seen with respect to the previous one. While the nodal displacement vector will be:

$$\{\mathbf{q}\} = \{u_{x1}\ u_{y1}\ u_{z1}\ \theta_{x1}\ \theta_{y1}\ \theta_{z1}\ u_{x2}\ u_{y2}\ u_{z2}\ \theta_{x2}\ \theta_{y2}\ \theta_{z2}\}'_{1\times12}$$

3.2 Time Integration: Newmark Scheme for dynamic study

Newmark is a second order accurate scheme to discretize a second order time system and perform integration in discrete time. It is applied to the following problem:

$$\begin{cases} \boldsymbol{M}\ddot{q} + \boldsymbol{C}\dot{q} + \boldsymbol{K}q = f(t) \\ q_0, \dot{q}_0 \qquad given \end{cases} \tag{3.1}$$

According to (M. Géradin, D. Rixen , 1997), we have the approximation formulas as:

$$\boxed{\begin{aligned} \dot{\boldsymbol{q}}_{n+1} &= \dot{\boldsymbol{q}}_n + (1-\gamma)h\ddot{\boldsymbol{q}}_n + \gamma h\ddot{\boldsymbol{q}}_{n+1} \\ \boldsymbol{q}_{n+1} &= \boldsymbol{q}_n + h\dot{\boldsymbol{q}}_n + h^2\left(\tfrac{1}{2}-\beta\right)\ddot{\boldsymbol{q}}_n + h^2\beta\ddot{\boldsymbol{q}}_{n+1} \end{aligned}} \tag{3.2}$$

While h is time step, and β and γ are parameters for which to ensure the stability we assign the following values:

$$\beta = \frac{1}{4} \quad \& \quad \gamma = \frac{1}{2}$$

In case, the dynamic equations (3.1) are linear, by introducing the scheme (3.2) in the equation of motion at time tn+1 we will have:

$$\begin{aligned} [\boldsymbol{M} + \gamma h\boldsymbol{C} + \beta h^2\boldsymbol{K}]\ddot{\boldsymbol{q}}_{n+1} = \boldsymbol{f}_{n+1} &- \boldsymbol{C}[\dot{\boldsymbol{q}}_n + (1-\gamma)h\ddot{\boldsymbol{q}}_n] \\ &- \boldsymbol{K}\left[\boldsymbol{q}_n + h\dot{\boldsymbol{q}}_n + (\tfrac{1}{2}-\beta)h^2\ddot{\boldsymbol{q}}_n\right] \end{aligned} \tag{3.3}$$

The matrix $[\boldsymbol{M} + \gamma h\boldsymbol{C} + \beta h^2\boldsymbol{K}]$ is iteration matrix, which due to properties of matrices **M**, **K,** and **C,** the iteration matrix is positive definite and symmetric.

A summary of the Newmark scheme for time integration of equation (3.1) is represented here as a flowchart. In prior, in the sake of more efficiency, we introduce the predictors $\dot{q}^*_{n+1}$ and q^*_{n+1}as:

$$\dot{\boldsymbol{q}}^*_{n+1} = \dot{\boldsymbol{q}}_n + (1-\gamma)h\ddot{\boldsymbol{q}}_n$$
$$\boldsymbol{q}^*_{n+1} = \boldsymbol{q}_n + h\dot{\boldsymbol{q}}_n + h^2(\tfrac{1}{2}-\beta)\ddot{\boldsymbol{q}}_n$$

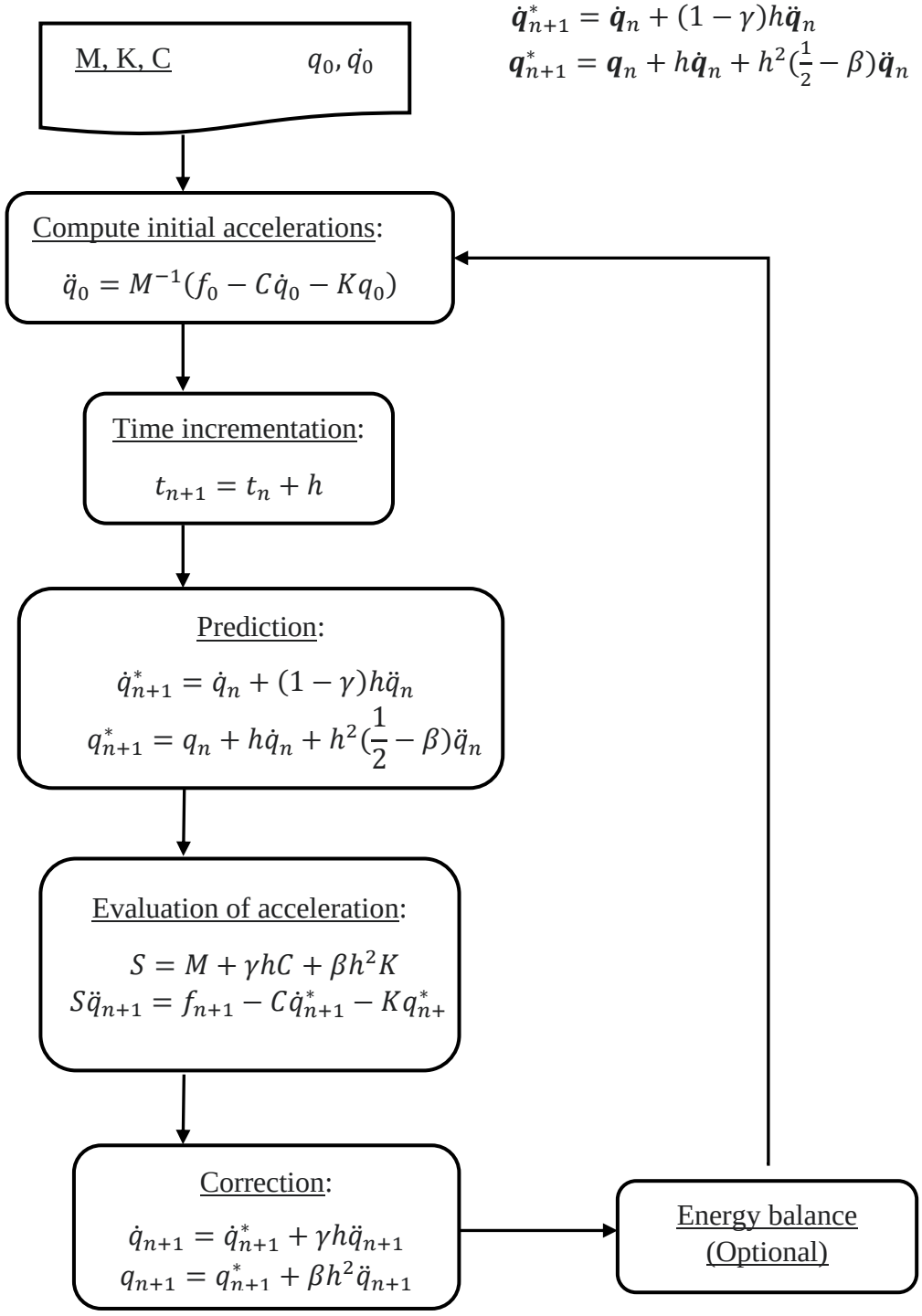

Figure 3.11 _ Flowchart – Newmark integration for linear systems

4 1st Configuration: Single-Span cable

The reference system we are going to simulate and study in this chapter is a single-span cable taut with a tensile load of T (pretension) and clamped at the two sides. But to prevent singularity in matrices, the axial displacement at the right-end side is free. The study consists of modal analysis, step response, harmonic response, and response to moving load. In the following the table 4.1 reports the geometrical data and some other properties of the systems.

Table 4.1 _ Geometrical data and parameters of the system

Density ρ 8940 kg/m3	mass per unit of length $\mu = \rho * \pi R^2$
Elastic modulus E 120 GP a	Span length l 6 m
Radius R $1.6 \cdot 10{-}2$ m	Force amplitude f0 20 kN
Pretension T 100 kN	Speed of the load v0 2 m/s

4.1 Implementation of E-B element

4.1.1 Global behavior of the beam

Now we are considering a beam with general orientation in space. In this case, we define a global reference of frame O (XYZ) so that the gravity field is directed toward the negative sign of the X-axis. In figure 4.1, a general beam with its local reference frame $\acute{O}$ and global reference frame O Is depicted.

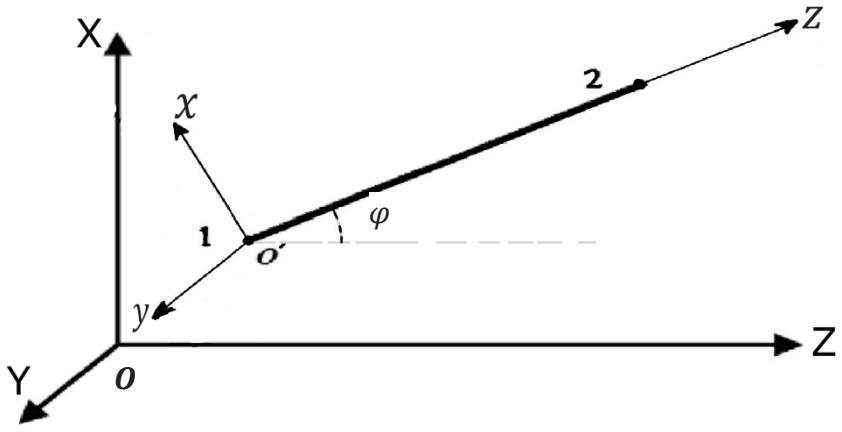

Figure 4.1 _ General E-B beam element with local and global reference frame respectively O and O'

We defined the global reference frame O (XYZ) and the local reference frame $\acute{O}$ (xyz) so that the beam locates on the XZ plane of the frame O, and the y-axis of frame $\acute{O}$ has the same direction as Y-axis in O frame. In this way, the beam has an inclination of angle φ with respect to axis Y. This logic will help us to drive the equation of motion of the beam with respect to the global reference frame.

The total expression of the mass and stiffness matrices associated with the adopted discretized element have a 12×12 size and will be as following:

$$\begin{bmatrix} ma_{1,1} & 0 & 0 & 0 & 0 & 0 & ma_{1,2} & 0 & 0 & 0 & 0 & 0 \\ 0 & mfx_{1,1} & 0 & 0 & 0 & mfx_{1,2} & 0 & mfx_{1,3} & 0 & 0 & 0 & mfx_{1,4} \\ 0 & 0 & mfy_{1,1} & 0 & mfy_{1,2} & 0 & 0 & 0 & mfy_{1,3} & 0 & mfy_{1,4} & 0 \\ 0 & 0 & 0 & mt_{1,1} & 0 & 0 & 0 & 0 & 0 & mt_{1,2} & 0 & 0 \\ 0 & 0 & mfy_{2,1} & 0 & mfy_{2,2} & 0 & 0 & 0 & mfy_{2,3} & 0 & mfy_{2,4} & 0 \\ 0 & mfx_{2,1} & 0 & 0 & 0 & mfx_{2,2} & 0 & mfx_{2,3} & 0 & 0 & 0 & mfx_{2,4} \\ ma_{2,1} & 0 & 0 & 0 & 0 & 0 & ma_{2,2} & 0 & 0 & 0 & 0 & 0 \\ 0 & mfx_{3,1} & 0 & 0 & 0 & mfx_{3,2} & 0 & mfx_{3,3} & 0 & 0 & 0 & mfx_{3,4} \\ 0 & 0 & mfy_{3,1} & 0 & mfy_{3,2} & 0 & 0 & 0 & mfy_{3,3} & 0 & mfy_{3,4} & 0 \\ 0 & 0 & 0 & mt_{2,1} & 0 & 0 & 0 & 0 & 0 & mt_{2,2} & 0 & 0 \\ 0 & 0 & mfy_{4,1} & 0 & mfy_{4,2} & 0 & 0 & 0 & mfy_{4,3} & 0 & mfy_{4,4} & 0 \\ 0 & mfx_{4,1} & 0 & 0 & 0 & mfx_{4,2} & 0 & mfx_{4,3} & 0 & 0 & 0 & mfx_{4,4} \end{bmatrix} \begin{Bmatrix} u_{z1} \\ u_{x1} \\ u_{y1} \\ \theta_{z1} \\ \theta_{x1} \\ \theta_{y1} \\ u_{z2} \\ u_{x2} \\ u_{y2} \\ \theta_{z2} \\ \theta_{x2} \\ \theta_{y2} \end{Bmatrix}$$

$$\{q\} = \{u_{z1}\ u_{x1}\ u_{y1}\ \theta_{z1}\ \theta_{x1}\ \theta_{y1}\ u_{z2}\ u_{x2}\ u_{y2}\ \theta_{z2}\ \theta_{x2}\ \theta_{y2}\}'_{1\times12}$$

In which $ma_{n,m}$ stands for elements in the M_A, $mt_{n,m}$ stands for elements in M_T, $mfx_{n,m}$ for elements in the M_{xz}, and $mfy_{n,m}$ for elements in M_{yz}.

Here is the complete mass matrix of the element is expressed and the same configuration holds for the total stiffness matrix of the element.

The complete expression for the nodal force vector for an inclined single beam element with respect to its local reference frame under pretension T is:

$$\boldsymbol{f} = \left\{\left(-T - \frac{pl}{2}\sin\varphi\right) \quad \frac{pl}{2}\cos\varphi \quad 0 \quad 0 \quad 0 \quad \frac{pl^2}{12}\cos\varphi \quad \left(T - \frac{pl}{2}\sin\varphi\right) \quad \frac{pl}{2}\cos\varphi \quad 0 \quad 0 \quad 0 \quad -\frac{pl^2}{12}\cos\varphi\right\}'_{1\times12}$$

Where T is the tensile load, $p = \mu g$ is the weight per unit length of the beam, and l is the length of the element.

As a result, the equation of motion of the element with respect to its local reference frame is as:

$$\boldsymbol{M}_l \ddot{\boldsymbol{q}}_l + \boldsymbol{K}_l \boldsymbol{q}_l = \boldsymbol{f}_l(t) \tag{4.1}$$

And $\boldsymbol{M}_l, \boldsymbol{C}_l$, and $\boldsymbol{K}_l$ are the mass, damping, and stiffness matrices of the element with respect to the local reference frame.

4.1.2 From local to global reference frame and rotation matrices

We can express the orientation of the local reference frame with respect to the global one by an appropriate rotation matrix, so that we can link the displacement vectors $q_{i_g}$and q_{i_l} which are respectively the displacement vector of the ith node in the global and local reference frames using coordinate transformation.

According to figure 4.1, the rotation matrix representing orientation local reference frame with respect to the global one is:

$$\boldsymbol{R} = \begin{bmatrix} \cos\varphi & \sin\varphi & 0 \\ -\sin\varphi & \cos\varphi & 0 \\ 0 & 0 & 1 \end{bmatrix}$$

The transformation can be expressed as:

$$\boldsymbol{q}_{i_l} = \boldsymbol{R}\boldsymbol{q}_{i_g} \tag{4.2}$$

In order to transfer the displacement vector of the element which has a dimension of 12×1, the expanded rotation matrix $\boldsymbol{R'}$ with a similar transformation is used. The expanded rotation matrix $\boldsymbol{R'}$ has a structure as the following:

$$\boldsymbol{R'} = \begin{bmatrix} [\boldsymbol{R}_{3\times3}] & [\boldsymbol{0}_{3\times3}] & [\boldsymbol{0}_{3\times3}] & [\boldsymbol{0}_{3\times3}] \\ [\boldsymbol{0}_{3\times3}] & [\boldsymbol{R}_{3\times3}] & [\boldsymbol{0}_{3\times3}] & [\boldsymbol{0}_{3\times3}] \\ [\boldsymbol{0}_{3\times3}] & [\boldsymbol{0}_{3\times3}] & [\boldsymbol{R}_{3\times3}] & [\boldsymbol{0}_{3\times3}] \\ [\boldsymbol{0}_{3\times3}] & [\boldsymbol{0}_{3\times3}] & [\boldsymbol{0}_{3\times3}] & [\boldsymbol{R}_{3\times3}] \end{bmatrix}_{12\times12}$$

To write the equation of the motion with respect to the global reference frame, we start from equation 4.1 which describes the behavior of the structure in the local reference frame. By implementing the transformation equation 4.2, we get:

$$\boldsymbol{R'^{-1}MR'\ddot{q}_g} + \boldsymbol{R'^{-1}KR'q_g} = \boldsymbol{f_g} \tag{4.3}$$

As the inverse of a rotation matrix is identical to its transpose, the global force vector, as well as the global mass and stiffness matrices can be expressed as:

$$\begin{aligned} \boldsymbol{M_g} &= \boldsymbol{R'^T M_l R'} \\ \boldsymbol{K_g} &= \boldsymbol{R'^T K_l R'} \\ \boldsymbol{f_g} &= \boldsymbol{R'^T f_l} \end{aligned} \tag{4.4}$$

4.1.3 Assembling and mapping matrices

After defining the elements mass and stiffness matrices in the local reference frame of the element, the global matrices must be assembled. The beam shown in the figure 4.1 has two symmetry planes in XZ and YZ plane and motion is supposed to be decoupled in XZ plane, YZ plane, axial displacement, and rotation along Z-axis.

In order to be able to illustrate more clearly, the beam, for example, can be discretized into three elements (1,2,3) and four nodes (1,2,3,4). The correct number of elements in the MATLAB code is much higher so that the global matrices' dimension will be of thousands.

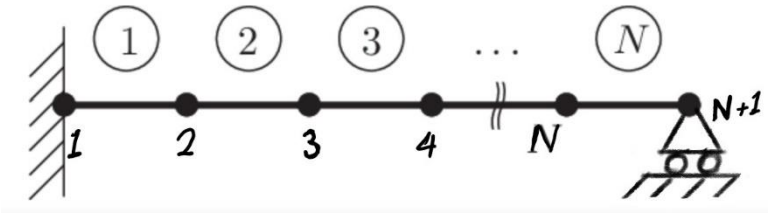

Figure 4.2 _ single-span cable modelled as a beam of N E-B elements

As it was discussed already, to each node are associated six DoFs. This means that the mass, stiffness and damping matrices associated to each discretized element have a 12×12 size while the global matrix of whole structure has a 24×24 size. The DoF arrangement will be:

$$\{q\} = \{u_{z1}\ u_{x1}\ u_{y1}\ \theta_{z1}\ \theta_{x1}\ \theta_{y1} \dots u_{z4}\ u_{x4}\ u_{y4}\ \theta_{z4}\ \theta_{x4}\ \theta_{y4}\}'_{1\times 24}$$

In general, a so-called Map Matrix that helps to move from elements to the whole structure. In our example with only three elements the map matrix would be the following:

Table 4.2 _ Assembling three elements of a single-span beam

	u_{z1} 1	u_{x1} 2	u_{y1} 3	θ_{z1} 4	θ_{x1} 5	θ_{y1} 6	u_{z2} 7	u_{x2} 8	u_{y2} 9	θ_{z2} 10	θ_{x2} 11	θ_{y2} 12	u_{z3} 13	u_{x3} 14	u_{y3} 15	θ_{z3} 16	θ_{x3} 17	θ_{y3} 18	...	θ_{x4} 23	θ_{y4} 24
1	u_{z1} 1	u_{x1} 2	u_{y1} 3	θ_{z1} 4	θ_{x1} 5	θ_{y1} 6	u_{z2} 7	u_{x2} 8	u_{y2} 9	θ_{z2} 10	θ_{x2} 11	θ_{y2} 12							...		
2							u_{z2} 1	u_{x2} 2	u_{y2} 3	θ_{z2} 3	θ_{x2} 4	θ_{y2} 5	u_{z3} 6	u_{x3} 7	u_{y3} 8	θ_{z3} 9	θ_{x3} 10	θ_{y3} 11	...		
3													u_{z3} 1	u_{x3} 2	u_{y3} 3	θ_{z3} 4	θ_{x3} 5	θ_{y3} 6	...	θ_{x4} 11	θ_{y4} 12

Once the mapping is done the global mass and stiffness matrix, in our example, can be built as:

$$\begin{bmatrix} \ddots & \vdots & \vdots & \vdots & \vdots & \vdots & \vdots & \vdots & \vdots & \vdots & \vdots & \vdots & \vdots \\ \cdots & \blacksquare & \blacksquare & \blacksquare & \blacksquare & \blacksquare & \blacksquare & \blacksquare & \blacksquare & 0 & 0 & 0 & \cdots \\ \cdots & \blacksquare & \blacksquare & \blacksquare & \blacksquare & \blacksquare & \blacksquare & \blacksquare & \blacksquare & 0 & 0 & 0 & \cdots \\ \cdots & \blacksquare & \blacksquare & \blacksquare+\blacksquare & \blacksquare+\blacksquare & \blacksquare+\blacksquare & \blacksquare+\blacksquare & \blacksquare+\blacksquare & \blacksquare+\blacksquare & \blacksquare & \blacksquare & \blacksquare & \cdots \\ \cdots & \blacksquare & \blacksquare & \blacksquare+\blacksquare & \blacksquare+\blacksquare & \blacksquare+\blacksquare & \blacksquare+\blacksquare & \blacksquare+\blacksquare & \blacksquare+\blacksquare & \blacksquare & \blacksquare & \blacksquare & \cdots \\ \cdots & \blacksquare & \blacksquare & \blacksquare+\blacksquare & \blacksquare+\blacksquare & \blacksquare+\blacksquare & \blacksquare+\blacksquare & \blacksquare+\blacksquare & \blacksquare+\blacksquare & \blacksquare & \blacksquare & \blacksquare & \cdots \\ \cdots & \blacksquare & \blacksquare & \blacksquare+\blacksquare & \blacksquare+\blacksquare & \blacksquare+\blacksquare & \blacksquare+\blacksquare & \blacksquare+\blacksquare & \blacksquare+\blacksquare & \blacksquare & \blacksquare & \blacksquare & \cdots \\ \cdots & \blacksquare & \blacksquare & \blacksquare+\blacksquare & \blacksquare+\blacksquare & \blacksquare+\blacksquare & \blacksquare+\blacksquare & \blacksquare+\blacksquare & \blacksquare+\blacksquare & \blacksquare & \blacksquare & \blacksquare & \cdots \\ \cdots & \blacksquare & \blacksquare & \blacksquare+\blacksquare & \blacksquare+\blacksquare & \blacksquare+\blacksquare & \blacksquare+\blacksquare & \blacksquare+\blacksquare & \blacksquare+\blacksquare & \blacksquare & \blacksquare & \blacksquare & \cdots \\ \cdots & 0 & 0 & \blacksquare & \blacksquare & \blacksquare & \blacksquare & \blacksquare & \blacksquare & \blacksquare & \blacksquare & \blacksquare & \cdots \\ \cdots & 0 & 0 & \blacksquare & \blacksquare & \blacksquare & \blacksquare & \blacksquare & \blacksquare & \blacksquare & \blacksquare & \blacksquare & \cdots \\ \cdots & 0 & 0 & \blacksquare & \blacksquare & \blacksquare & \blacksquare & \blacksquare & \blacksquare & \blacksquare & \blacksquare & \blacksquare & \cdots \\ \cdots & \vdots & \vdots & \vdots & \vdots & \vdots & \vdots & \vdots & \vdots & \vdots & \vdots & \vdots & \ddots \end{bmatrix} \begin{Bmatrix} \vdots \\ \theta_{x1} \\ \theta_{y1} \\ u_{z2} \\ u_{x2} \\ u_{y2} \\ \theta_{z2} \\ \theta_{x2} \\ \theta_{y2} \\ u_{z3} \\ u_{x3} \\ u_{y3} \\ \vdots \end{Bmatrix}$$

Where:

■: Represent certain entry at that position.

■+■: Represents the additions to the matrix entries when the sub matrices overlap.

The global mass and stiffness matrices of the whole structure $\boldsymbol{M}_T$ and $\boldsymbol{K}_T$ and the global nodal force vector $\boldsymbol{f}_T(t)$ are achieved by this assembling approach. In the picture below, the final structure of the total stiffness matrix of the structure is depicted which is identical to that of the total mass matrix.

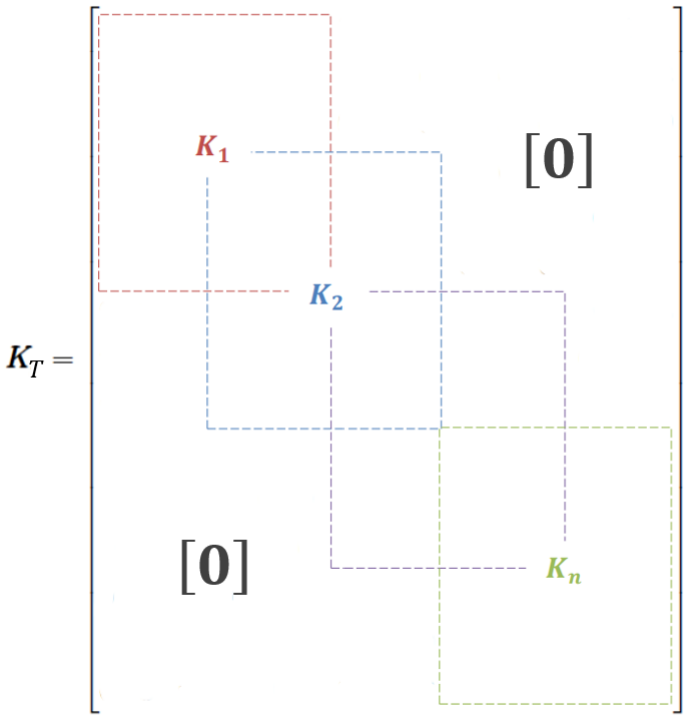

Figure 4.3 _ Total stiffness matrix of the structure configuration

As a result, the global equation of motion of the entire structure is:

$$\boldsymbol{M}_T\ddot{\boldsymbol{q}} + \boldsymbol{K}_T\boldsymbol{q} = \boldsymbol{f}_T(t) \tag{4.5}$$

From this moment on, vector $\boldsymbol{q}$ represents the global nodal displacement vector of the whole structure.

Now that we have written the equation of motion and mass and stiffness matrices of the whole structure with respect to the global reference frame, the possibility of introducing damping effect can be considered adopting the proportional damping matrix $\boldsymbol{C}_T$ as following:

$$\boldsymbol{C}_T = \alpha \boldsymbol{M}_T + \beta \boldsymbol{K}_T \tag{4.6}$$

Then the equation of motion will become:

$$\boldsymbol{M}_T \ddot{\boldsymbol{q}} + \boldsymbol{C}_T \dot{\boldsymbol{q}} + \boldsymbol{K}_T \boldsymbol{q} = \boldsymbol{f}_T(t) \tag{4.7}$$

4.2 Boundary Conditions and Static equilibrium

Due to the presence of the clamped constraint at the starting node and blocking all the degrees of freedom except for the axial displacement at the ending node for the sake of preventing singular matrices, as a result, almost null displacement and rotation occur at those DoF's. In our example:

$$\{q_1\} = \begin{Bmatrix} u_{z1} \\ u_{x1} \\ u_{y1} \\ \theta_{z1} \\ \theta_{x1} \\ \theta_{y1} \end{Bmatrix} = \begin{Bmatrix} 0 \\ 0 \\ 0 \\ 0 \\ 0 \\ 0 \end{Bmatrix} \qquad \{q_4\} = \begin{Bmatrix} u_{z1} \\ u_{x1} \\ u_{y1} \\ \theta_{z1} \\ \theta_{x1} \\ \theta_{y1} \end{Bmatrix} = \begin{Bmatrix} u_{z1} \\ 0 \\ 0 \\ 0 \\ 0 \\ 0 \end{Bmatrix}$$

There are two approaches to implement the constraints. The first solution is to reduce the dimension of both global mass and global stiffness matrices of the structure by cancelling the corresponding rows and columns of the constrained degrees of freedom. Advantage of this approach is a quick and easy numerical simulation, but on the other hand it could not represent the reality of the constraints. Since, however a constraint blocks a DoF, but that DoF would still have a small displacement.

The second solution enables the simulation to be closer to the reality. In this approach, instead of cancelling any DoFs, we introduce strong relevant stiffness at that DoF. The selected value for this additional stiffness must represent infinity compared to other related stiffness values. This method still has its own disadvantages.

By adding high values of stiffnesses, practically we introduce very high values of frequencies to the system, numerically point of view, time step will be extremely small, and this makes very expensive simulation in the matter of time.

Adopting the second solution, k and χ are nomination for added stiffnesses implementing respectively on translational and rotational DoFs. For instance, χ_{z1} is the added translational stiffness to the torsion about z direction (the axis of the beam) at the first node. As a result, all the additional stiffnesses are as the following:

$$\{k_{z1}\ \ k_{x1}\ \ k_{y1}\ \ \chi_{z1}\ \ \chi_{x1}\ \ \chi_{y1}\ \ k_{x4}\ \ k_{y4}\ \ \chi_{z4}\ \ \chi_{x4}\ \ \chi_{y4}\}$$

Incrementation of potential energy due to additional stiffnesses is:

$$\Delta U = \frac{1}{2}k_{z1}(u_{z1})^2 + \frac{1}{2}k_{x1}(u_{x1})^2 + \frac{1}{2}k_{y1}\left(u_{y1}\right)^2 + \frac{1}{2}\chi_{z1}(\theta_{z1})^2 + \frac{1}{2}\chi_{x1}(\theta_{x1})^2 + \frac{1}{2}\chi_{y1}\left(\theta_{y1}\right)^2 + \cdots$$
$$\ldots + \tfrac{1}{2}k_{x4}(u_{x4})^2 + \tfrac{1}{2}k_{y4}\left(u_{y4}\right)^2 + \tfrac{1}{2}\chi_{z4}(\theta_{z4})^2 + \tfrac{1}{2}\chi_{x4}(\theta_{x4})^2 + \tfrac{1}{2}\chi_{y4}\left(\theta_{y4}\right)^2$$

The stiffnesses representing the boundary conditions will modify global stiffness matrix:

$$\frac{d}{dt}\left(\frac{\partial \Delta U}{\partial u_{z1}}\right) = k_{z1}u_{z1} \qquad \frac{d}{dt}\left(\frac{\partial \Delta U}{\partial u_{z4}}\right) = k_{z4}u_{z4}$$

$$\frac{d}{dt}\left(\frac{\partial \Delta U}{\partial u_{x1}}\right) = k_{x1}u_{x1} \qquad \frac{d}{dt}\left(\frac{\partial \Delta U}{\partial u_{y4}}\right) = k_{y4}u_{y4}$$

$$\frac{d}{dt}\left(\frac{\partial \Delta U}{\partial u_{y1}}\right) = k_{y1}u_{y1} \qquad \frac{d}{dt}\left(\frac{\partial \Delta U}{\partial \theta_{z4}}\right) = \chi_{z4}\theta_{z4}$$

$$\frac{d}{dt}\left(\frac{\partial \Delta U}{\partial \theta_{z1}}\right) = \chi_{z1}\theta_{z1} \qquad \frac{d}{dt}\left(\frac{\partial \Delta U}{\partial \theta_{x4}}\right) = \chi_{x4}\theta_{x4}$$

$$\frac{d}{dt}\left(\frac{\partial \Delta U}{\partial \theta_{x1}}\right) = \chi_{x1}\theta_{x1} \qquad \frac{d}{dt}\left(\frac{\partial \Delta U}{\partial \theta_{y4}}\right) = \chi_{y4}\theta_{y4}$$

$$\frac{d}{dt}\left(\frac{\partial \Delta U}{\partial \theta_{y1}}\right) = \chi_{y1}\theta_{y1}$$

Since in our case the added stiffnesses link the corresponding DoFs to the ground not another DoFs, these values are added to the relative array on the main diagonal of stiffness matrix:

$$\begin{bmatrix} \blacksquare + k_{z1} & \blacksquare & \blacksquare & \blacksquare & \blacksquare & \blacksquare & \cdots & 0 & 0 \\ \blacksquare & \blacksquare + k_{x1} & \blacksquare & \blacksquare & \blacksquare & \blacksquare & \cdots & 0 & 0 \\ \blacksquare & \blacksquare & \blacksquare + k_{y1} & \blacksquare & \blacksquare & \blacksquare & \cdots & 0 & 0 \\ \blacksquare & \blacksquare & \blacksquare & \blacksquare + \chi_{z1} & \blacksquare & \blacksquare & \cdots & 0 & 0 \\ \blacksquare & \blacksquare & \blacksquare & \blacksquare & \blacksquare + \chi_{x1} & \blacksquare & \cdots & 0 & 0 \\ \blacksquare & \blacksquare & \blacksquare & \blacksquare & \blacksquare & \blacksquare + \chi_{y1} & \cdots & 0 & 0 \\ \vdots & \vdots & \vdots & \vdots & \vdots & \vdots & \ddots & \vdots & \vdots \\ 0 & 0 & 0 & 0 & 0 & 0 & \cdots & \blacksquare + \chi_{x4} & \blacksquare \\ 0 & 0 & 0 & 0 & 0 & 0 & \cdots & \blacksquare & \blacksquare + \chi_{y4} \end{bmatrix} \begin{Bmatrix} u_{z1} \\ u_{x1} \\ u_{y1} \\ \theta_{z1} \\ \theta_{x1} \\ \theta_{y1} \\ \vdots \\ \theta_{x24} \\ \theta_{y24} \end{Bmatrix}$$

4.2.1 Calculation of Static equilibrium and Reaction Forces

The static displacement of the system due to weight of the cable can easily be calculated by solving:

$$\boldsymbol{K}_T \boldsymbol{q}_S = \boldsymbol{f}_T \qquad \rightarrow \qquad \boldsymbol{q}_S = \boldsymbol{K}_T^{-1} \boldsymbol{f}_T \tag{4.8}$$

The displacement calculated using this approach, matches perfectly the one which achieved adopting the continuous method in previous works. Figure 4.4 below represents the static equilibrium obtained in this way.

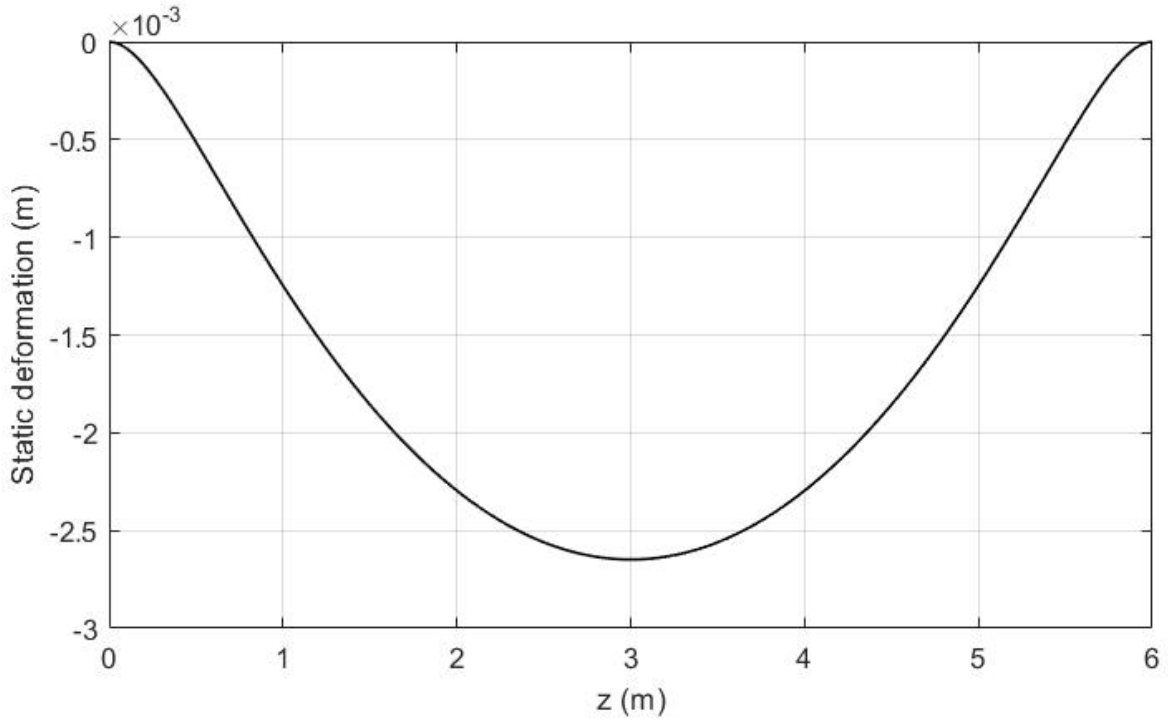

Figure 4.4 _ Static equilibrium

Reaction forces at the boundaries:

To calculate reaction forces at boundaries, there are two approaches that rely on the method which has been implemented to introduce the boundary conditions:

As the first approach, if the constraints have been introduced by canceling the corresponding rows and columns, we can obtain the reaction forces simply by following these steps:

By canceling only the columns and not the rows of the stiffness matrix corresponding to those DOFs that have been constrained and eliminating the displacement of those DOFs from the displacement vector, since they are equal to zero, and finally by multiplying the remaining sub-matrix of the stiffness matrix to the remaining sub-vector of the displacement vector, we can obtain our result.

As we have defined the constrained DOFs by adding strong relevant stiffness values to the corresponding elements of the stiffness matrix, The second approach is implemented as follow:

Since in this case, although the concerned DOFs are constrained but still have small displacements, so by multiplying these small displacements to their corresponding stiffness values, we can calculate the reaction forces. This method is adopted in this work.

With respect to our example described so far, we have:

$$F_{z1} = k_{z1}u_{z1} \qquad F_{x2} = k_{x2}u_{x2}$$
$$F_{x1} = k_{x1}u_{x1} \qquad F_{y2} = k_{y2}u_{y2}$$
$$F_{y1} = k_{y1}u_{y1} \qquad M_{z2} = \chi_{z2}\theta_{z2}$$
$$M_{z1} = \chi_{z1}\theta_{z1} \qquad M_{x2} = \chi_{x2}\theta_{x2}$$
$$M_{x1} = \chi_{x1}\theta_{x1} \qquad M_{y2} = \chi_{y2}\theta_{y2}$$
$$M_{y1} = \chi_{y1}\theta_{y1}$$

The displacement vector can be either static configuration or dynamic behavior. Later we will see by imposing the excitation loads to the system, by using this logic we can calculate the variation of reaction forces over time.

4.3 Modal analysis of the system and validation

In the following, the figures depict the first five modes of the system in the vertical direction.

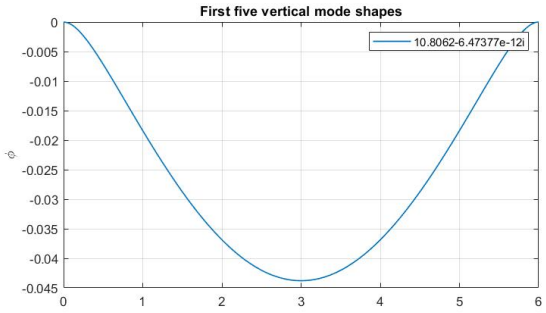

Figure 4.8 _ 1st vertical mode shape

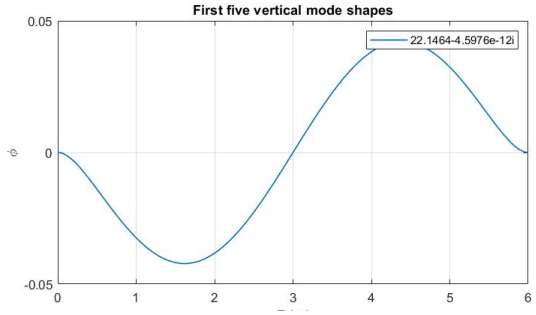

Figure 4.7 _ 2nd vertical mode shape

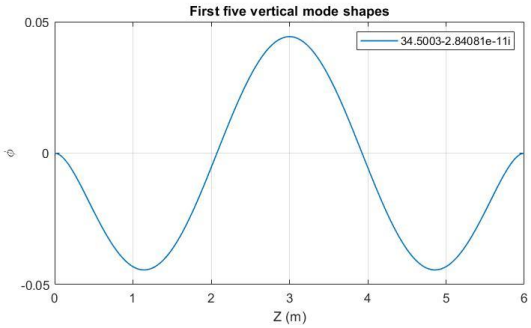

Figure 4.6 _ 3rd vertical mode shape

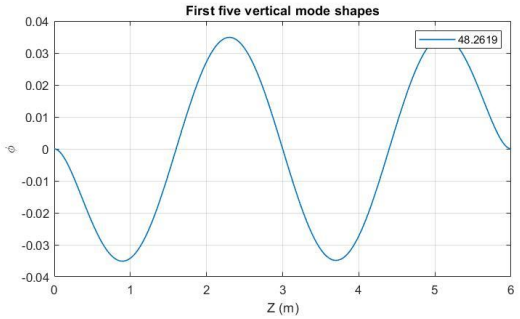

Figure 4.5 _ 4th vertical mode shape

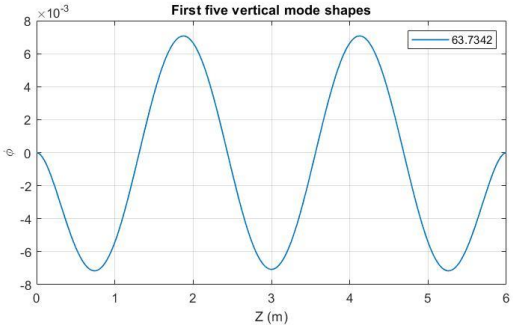

Figure 4.9 _ 5th vertical mode shape

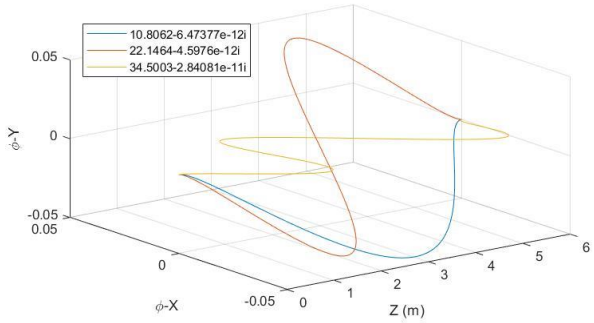

Figure 4.10 _ The first 3 vertical modes in 3D space

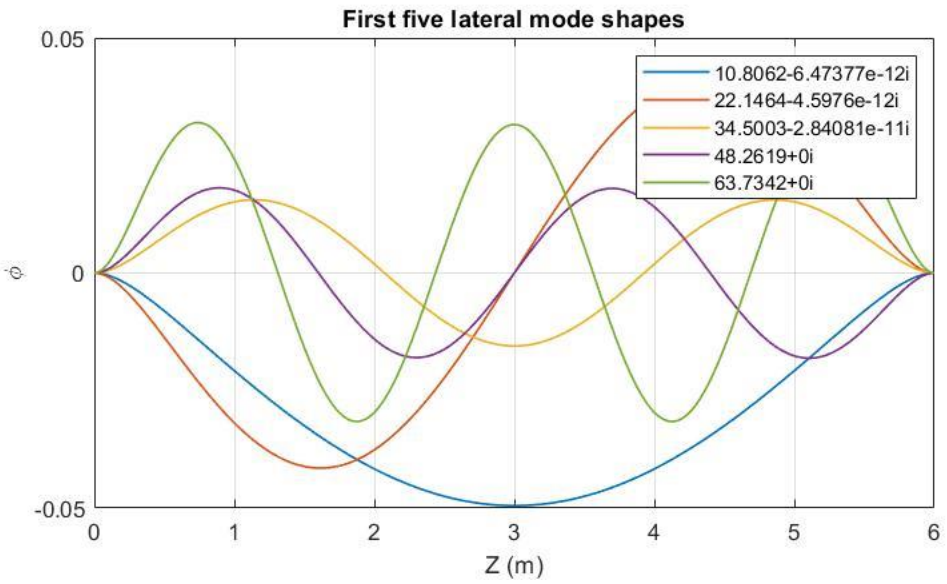

Figure 4.11 _ The first five modes in lateral direction

As we can see from the table 4.3 and figure 4.11, the modes in lateral direction (Y-axis) are identical to those in vertical direction (X-axis) and that is because the beam element is axisymmetric, prismatic homogeneous.

Table 4.3 _ Natural frequency values (Hz)

Direction	First mode (Hz)	Second mode (Hz)	Third mode (Hz)	Forth mode (Hz)	Fifth mode (Hz)
Vertical – along X	10.8062	22.1464	34.5003	48.2619	63.7342
Lateral – along Y	10.8062	22.1464	34.5003	48.2619	63.7342

4.4 Dynamic responses of the system

The equation of motion which represents the dynamic behavior of the system is:

$$\boldsymbol{M}_T\ddot{\boldsymbol{q}} + \boldsymbol{C}_T\dot{\boldsymbol{q}} + \boldsymbol{K}_T\boldsymbol{q} = \boldsymbol{f}_T(t) \tag{4.7}$$

In which we have considered the proportional damping effect:

$$\boldsymbol{C}_T = \alpha\boldsymbol{M}_T + \beta\boldsymbol{K}_T \tag{4.6}$$

In order to introduce the effect of damping to the response of the system, we need to set parameters α and β different from zero. As a result, our dynamic simulations have been performed with $\alpha = 0$ and $\beta = 1e^{-4}$. In this way, we can see that intension of the system over time is to settle on the static equilibrium.

The dynamic study is performed in a discrete time manner, and in this regard, we set the time step $dt = 0.5e^{-3}s$.

With respect to time integration, as it was discussed earlier, we adopt Newmark scheme. Since we study the dynamic behavior of the system with respect to static equilibrium, as the initial condition to the Newmark method $q_0, \dot{q}_0$, we set:

$$\boldsymbol{q}_0 = \boldsymbol{q}_s \quad \& \quad \dot{\boldsymbol{q}}_0 = \{\boldsymbol{0}\}$$

In which $\boldsymbol{q}_s$ is the static equilibrium we obtained by equation 4.7

4.4.1 Step Response

In this case, the excitation force is a step function along with the negative sign of the X-axis, which acts on the system at $t = 0s$ and vanishes at time $t = 2s$ as below:

$$f(t) = \begin{cases} 0, & t < 0 \\ F_0, & 0 \leq t \leq 2 \\ 0, & t \geq 2 \end{cases}$$

In which $F_0 = -20\ kN$ and the load is applied on the cable at a node which is located on $z = 4m$.

The nodal force vector of the node which is subjected to the load would be expressed as the following vector:

$$\boldsymbol{f}_n = \{0 \quad f(t) \quad 0 \quad 0 \quad 0 \quad 0\}$$

Step excitation is like an act of changing the static equilibrium to a new one at time t, and the response is a kind of transient free response about the new equilibrium condition.

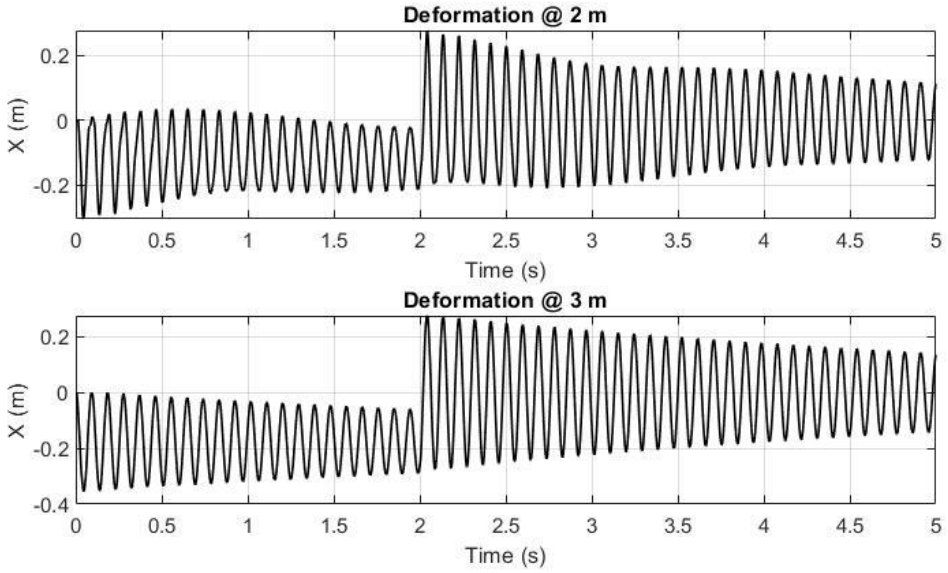

Figure 4.12 _ The response of the system to step function

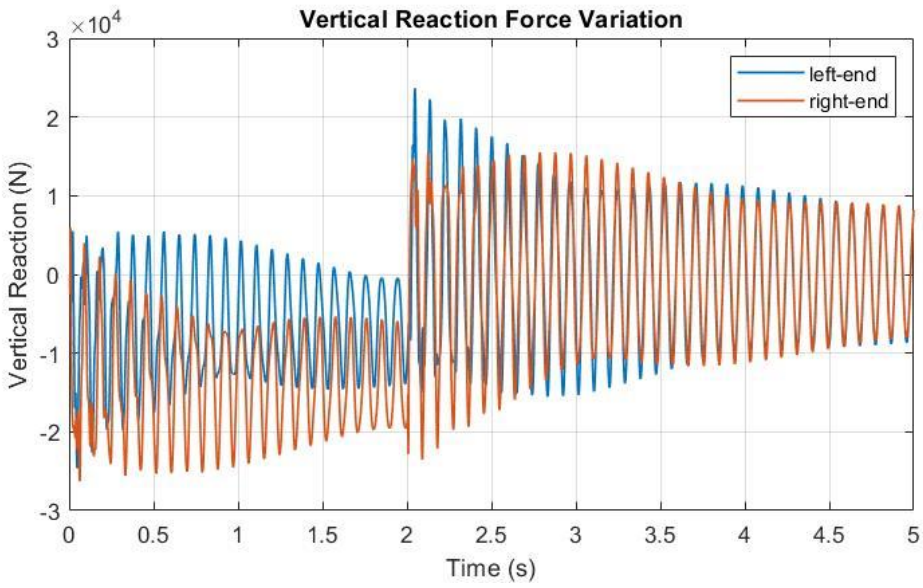

Figure 4.13 _ The vertical reaction forces of the constraints

Figure .12 depicts the time history of displacements of two points which are located at $Z = 2m$ and $Z = 3m$. As well as figure 4.13 displays the time history of variation of the constraint reaction alongside the vertical direction.

4.4.2 Harmonic Response

To study the harmonic response of the system, we have excited the system by imposing harmonic load on a specific node located at $Z = 4m$.

$$f(t) = F_0 \sin(2\pi\varphi t)$$

In which $F_0 = 20\ kN$, and φ is the frequency in Hz.

As what we have seen, the nodal force vector of the node which is subjected to the load would be expressed as the following vector:

$$\boldsymbol{f}_n = \{0 \quad f(t) \quad 0 \quad 0 \quad 0 \quad 0\}$$

The first natural frequency of the system is φ_1 *=10.8062 Hz*, and the frequency of the harmonic load is set close to it, $\varphi = 10\ Hz$.

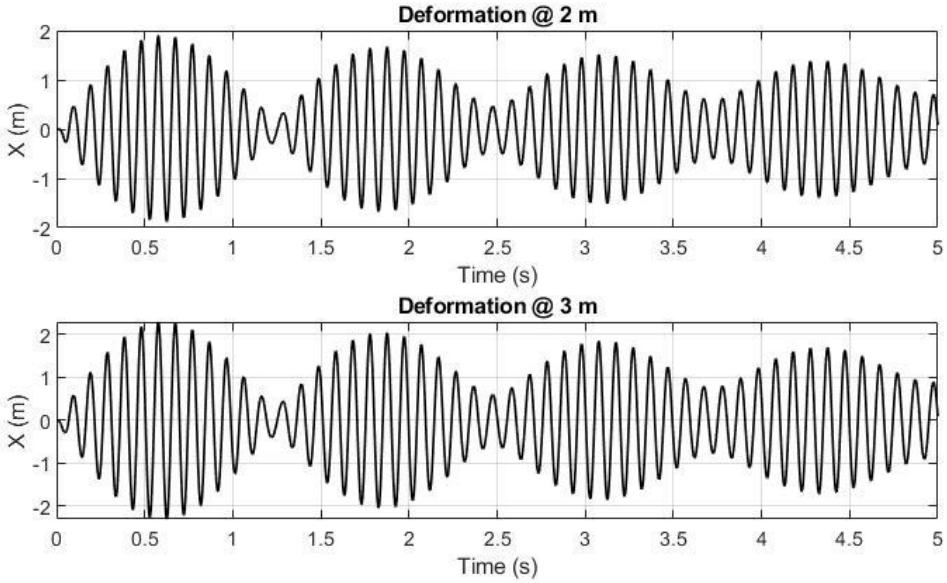

Figure 4.14 _ Harmonic response of the system at two points

Since the frequency of excitation is close the natural frequency, the so-called beating effect occurs which can be noticed in figure 4.14 which displays the time history of displacements of two nodes of the cable at $Z = 2m$ and $Z = 3m$.

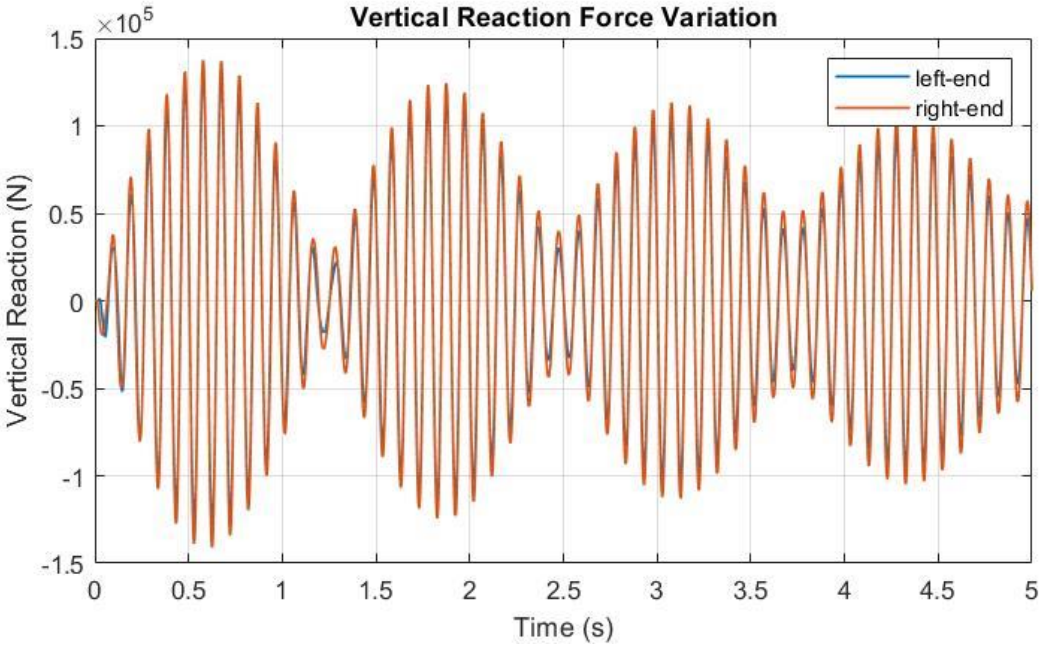

Figure 4.15 _ The vertical reaction forces of the constraints due to harmonic excitation

4.4.3 Response to moving load

The first challenge to simulate a ropeway is to model a moving load as a representative to the cabin passing through the cable. We can model a moving ropeway carrying cabins attached to it, by considering a fixed and stationary cable subjected to a moving load.

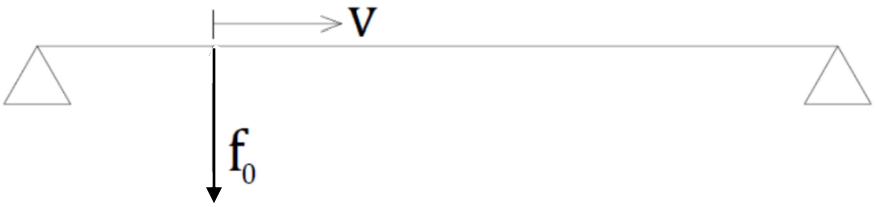

Figure 4.16 _ Scheme of the system under analysis

In this case, a very important point to consider is that since the load position changes in each time increment, as a result, in order to have a smooth movement of load through the entire cable and not only on the nodes, it is possible to consider the distribution of the load on each element using shape function matrix $[N]$ which is a function of space ($\zeta = \frac{z}{l}$).

$$\boldsymbol{f} = [N]^T f_0 \tag{4.9}$$

With respect to Euler-Bernoulli beam element, the shape function matrix is:

$$[N] = \begin{bmatrix} N_{a1} & 0 & 0 & 0 & 0 & 0 & N_{a2} & 0 & 0 & 0 & 0 & 0 \\ 0 & N_{f_{1,1}} & 0 & 0 & 0 & N_{f_{1,2}} & 0 & N_{f_{1,3}} & 0 & 0 & 0 & N_{f_{1,4}} \\ 0 & 0 & N_{f_{1,1}} & 0 & -N_{f_{1,2}} & 0 & 0 & 0 & N_{f_{1,3}} & 0 & -N_{f_{1,4}} & 0 \\ 0 & 0 & 0 & N_{t1} & 0 & 0 & 0 & 0 & 0 & N_{t2} & 0 & 0 \\ 0 & 0 & -N_{f_{2,1}} & 0 & N_{f_{2,2}} & 0 & 0 & 0 & -N_{f_{2,3}} & 0 & N_{f_{2,4}} & 0 \\ 0 & N_{f_{2,1}} & 0 & 0 & 0 & N_{f_{2,2}} & 0 & N_{f_{2,3}} & 0 & 0 & 0 & N_{f_{2,4}} \end{bmatrix}$$

In which $N_a, N_f, and\ N_t$ are elements of shape function matrices in respectively axial, flexural, and torsional behavior that we already introduced them on chapter 3.1.1, and they are functions of ($\zeta = \frac{z}{l}$).

At each time increment dt, these shape functions must be evaluated at the exact position at time t where the load is located. In this regard, we substitute the value:

$$z = v_0 t \qquad \rightarrow \qquad \zeta = \frac{v_0 t}{l}$$

In the equation (4.9).

Results

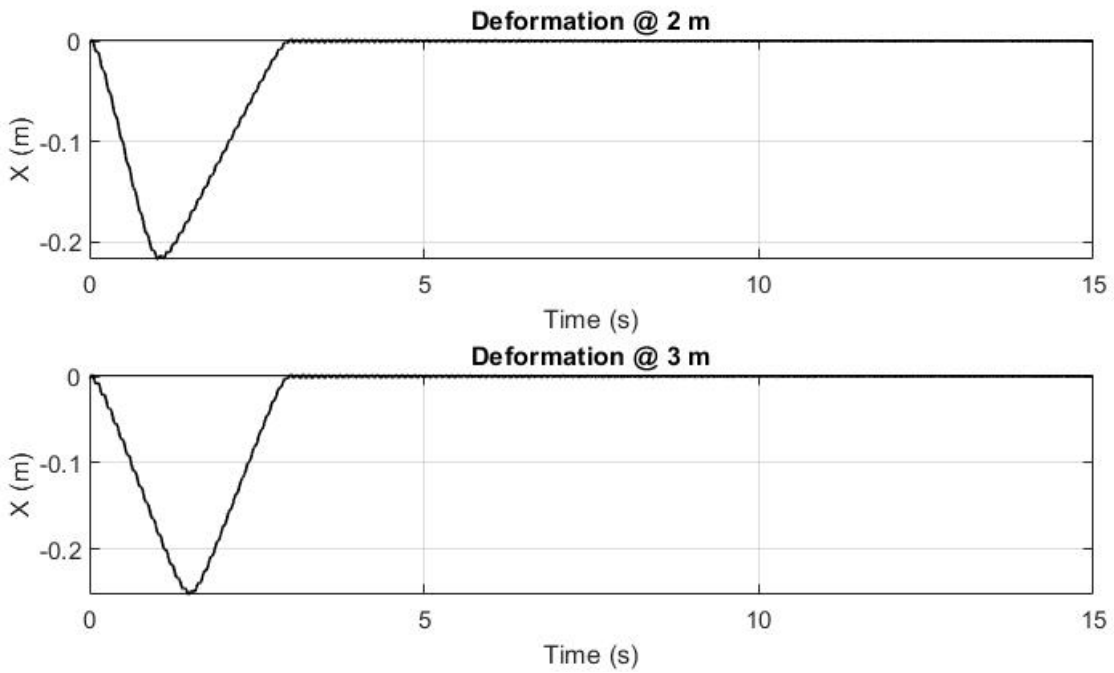

Figure 4.17 _ Time history of displacement at two points

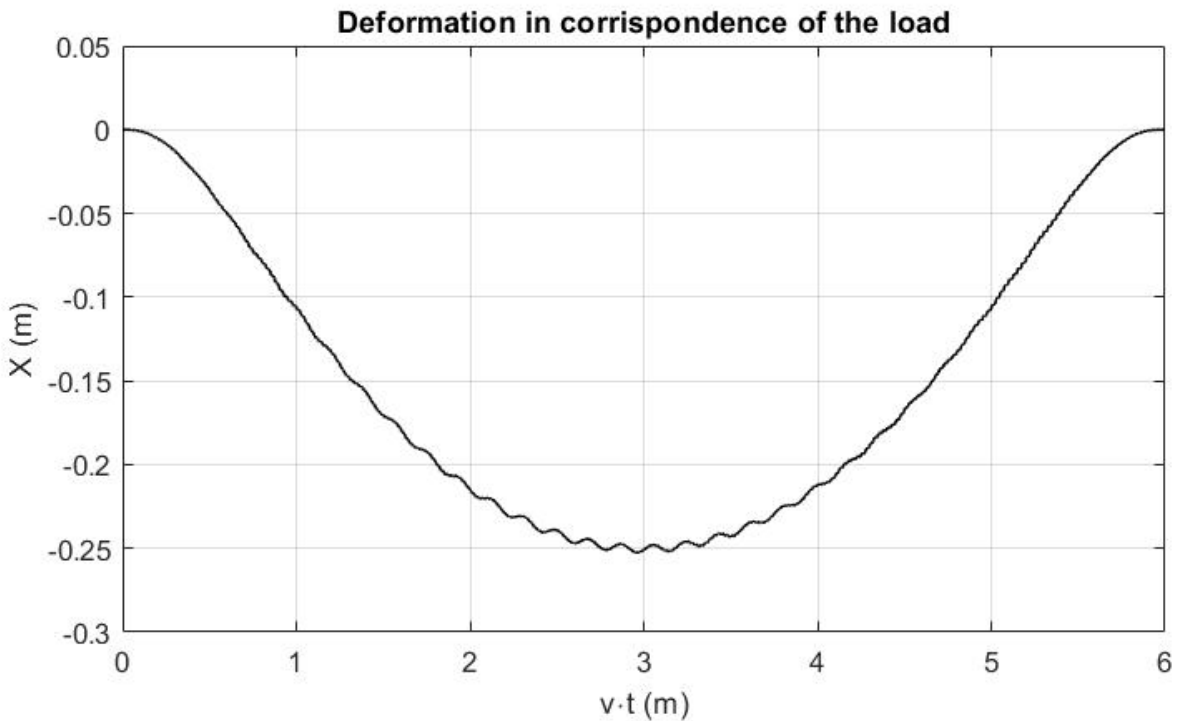

Figure 4.18 _ Deformation of the cable with correspondence of the load

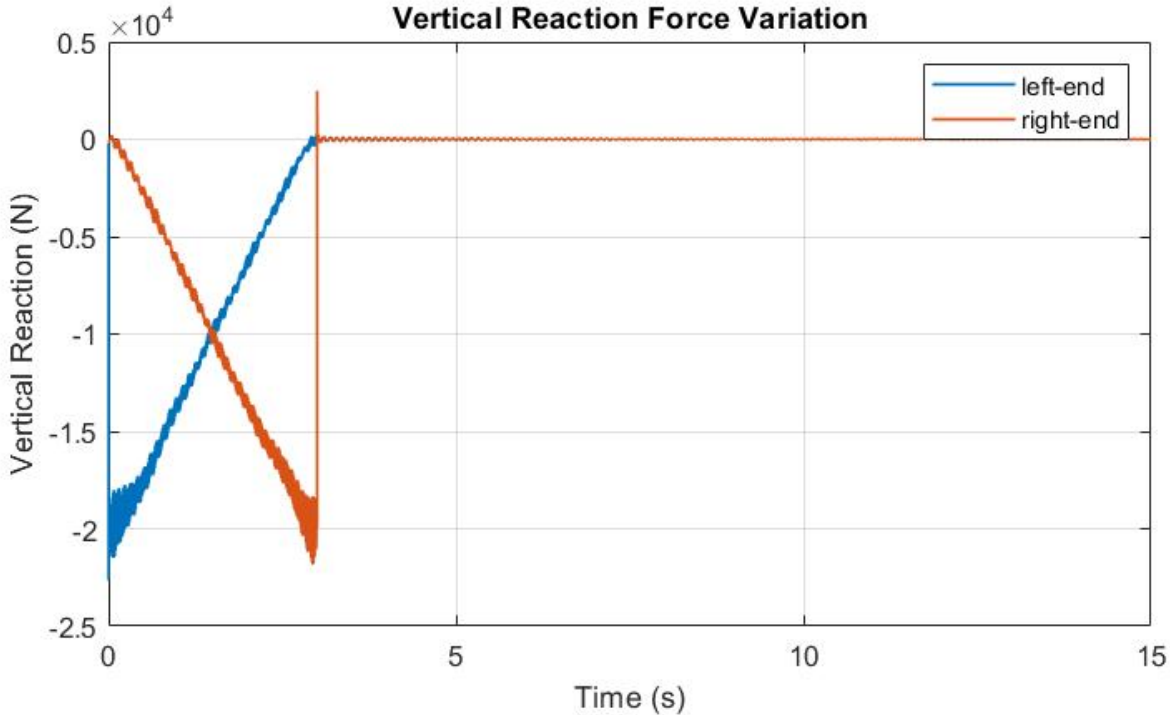

Figure 4.19 _ The variation of the vertical reaction forces over time

Considering a time integration intervals five time larger than what is takes for load to pass through the entire span, i.e. $0 \leq t \leq 5L/v_0$, we will have the possibility to analyze also the transient deformation of the cable toward the static equilibrium after the reaches the ending point.

Plotting the time history of the displacement of some points (figure 4.17) would be helpful to observe how the cable oscillates.

The damped oscillations displayed so far, are in accordance with our expectation approve the reliability and correctness of the model.

5 2nd Configuration: Multi-Span cable

The discretization Euler-Bernoulli beam element and the Newmark scheme have been used successfully to model single-span beam. To advance our simulation, these methods are utilized to study the multi-span cable. We start with a two-span beam with the following information:

Table 5.1 _ Geometrical data and parameters of the system

Density ρ 8940 kg/m3	mass per unit of length $\mu = \rho * \pi R^2$
Elastic modulus E 120 GP a	Span length 1 l 10 m
Radius R $1.6 \cdot 10{-}2$ m	Span length 2 l 8 m
Force amplitude f0 2 kN	Speed of the load v0 2 m/s

In this case, pretention $T = 0$.

5.1 Implementation of E-B element,

5.1.1 From local to global reference frame and rotation matrices

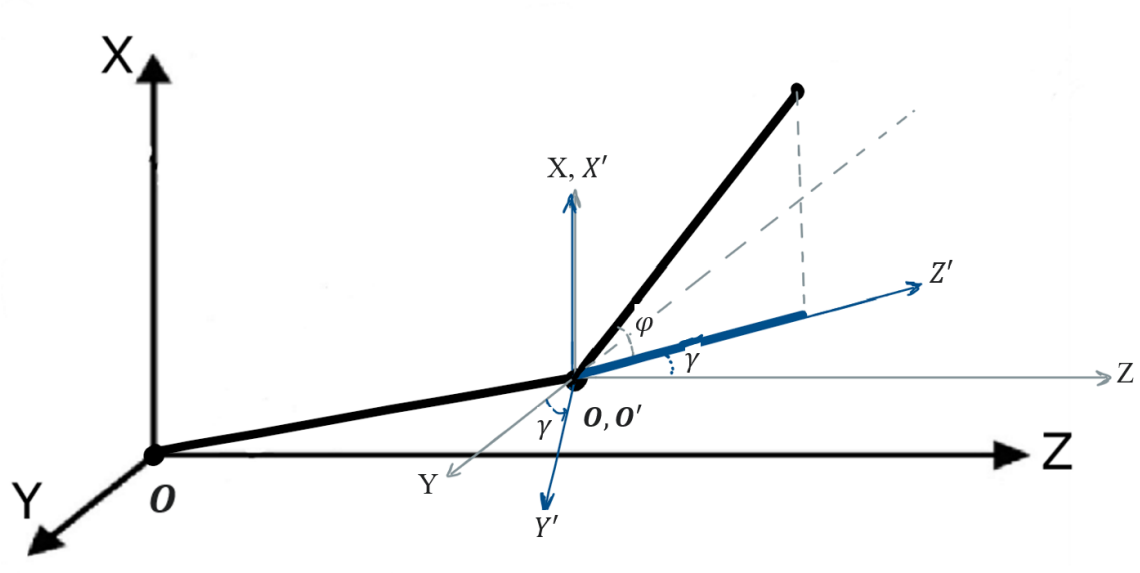

Figure 5.1_ General orientation of beam in space

In figure 5.1, a two-span beam with general orientations in space is displayed. In this case, similarly, the global reference of frame O (XYZ) is defined so that the gravity field is directed toward the negative sign of the X-axis and the first span of the beam is in the XZ plane.

On the second beam, an intermediate reference frame O' ($X'Y'Z'$) is introduced so that the beam locates on the $X'Z'$ plane of the frame O', and the X'-axis of frame O' has the same direction as X-axis in the O frame. In this way, the beam has an inclination of angle φ with respect to axis Y' and angle γ with respect to axis X. This logic will help us to drive the equation of motion of the beam with respect to the global reference frame using an adequate two-step transformation equation.

To link the displacement vectors q_{i_g} and q_{i_l} which are respectively the displacement vector of the ith node with respect to the global and local reference frames, first we need to introduce a coordinate transformation from intermediate frame to local one, and then from global to intermediate reference frame. Considering the fact that the local reference frame is the one with respect to which, we derived the matrices and the $z - axis$ coincides with the axial direction of the beam.

$1st$: Transformation from intermediate reference frame O' to the local one:

$$\boldsymbol{R}_{\varphi} = \begin{bmatrix} \cos\varphi & \sin\varphi & 0 \\ -\sin\varphi & \cos\varphi & 0 \\ 0 & 0 & 1 \end{bmatrix}$$

The corresponding transformation can be expressed as:

$$\boldsymbol{q}_{i_l} = \boldsymbol{R}_{\varphi}\boldsymbol{q}_{i_{int}} \tag{5.1}$$

$2nd$: Transformation from global reference frame O to the intermediate one O':

$$\boldsymbol{R}_{\gamma} = \begin{bmatrix} \cos\gamma & 0 & -\sin\gamma \\ 0 & 1 & 0 \\ \sin\gamma & 0 & \cos\gamma \end{bmatrix}$$

And the corresponding transformation can be expressed as:

$$\boldsymbol{q}_{i_{int}} = \boldsymbol{R}_{\gamma}\boldsymbol{q}_{i_g} \tag{5.2}$$

As a result, the direct transformation from global to local reference frame is conducted by the following rotation matrix and transformation expression:

$$\boldsymbol{R} = \boldsymbol{R}_{\varphi} \times \boldsymbol{R}_{\gamma} \qquad \rightarrow \qquad \boldsymbol{q}_{i_l} = \boldsymbol{R}\boldsymbol{q}_{i_g} \tag{5.3}$$

Again, the expanded rotation matrix $\boldsymbol{R'}$ would be:

$$\boldsymbol{R'} = \begin{bmatrix} [\boldsymbol{R}_{3\times3}] & [\boldsymbol{0}_{3\times3}] & [\boldsymbol{0}_{3\times3}] & [\boldsymbol{0}_{3\times3}] \\ [\boldsymbol{0}_{3\times3}] & [\boldsymbol{R}_{3\times3}] & [\boldsymbol{0}_{3\times3}] & [\boldsymbol{0}_{3\times3}] \\ [\boldsymbol{0}_{3\times3}] & [\boldsymbol{0}_{3\times3}] & [\boldsymbol{R}_{3\times3}] & [\boldsymbol{0}_{3\times3}] \\ [\boldsymbol{0}_{3\times3}] & [\boldsymbol{0}_{3\times3}] & [\boldsymbol{0}_{3\times3}] & [\boldsymbol{R}_{3\times3}] \end{bmatrix}_{12\times12}$$

As what we have seen in section 4.1.2, the equation of the motion with respect to the global reference frame is:

$$\boldsymbol{R'}^{T}\boldsymbol{M}\boldsymbol{R'}\ddot{\boldsymbol{q}}_g + \boldsymbol{R'}^{T}\boldsymbol{K}\boldsymbol{R'}\boldsymbol{q}_g = \boldsymbol{f}_g \tag{5.4}$$

And the global matrices and vector associated with one element is:

$$\begin{aligned} \boldsymbol{M}_g &= \boldsymbol{R'}^{T}\boldsymbol{M}_l\boldsymbol{R'} \\ \boldsymbol{K}_g &= \boldsymbol{R'}^{T}\boldsymbol{K}_l\boldsymbol{R'} \\ \boldsymbol{f}_g &= \boldsymbol{R'}^{T}\boldsymbol{f}_l \end{aligned} \tag{5.5}$$

5.1.2 Assembling and mapping matrices

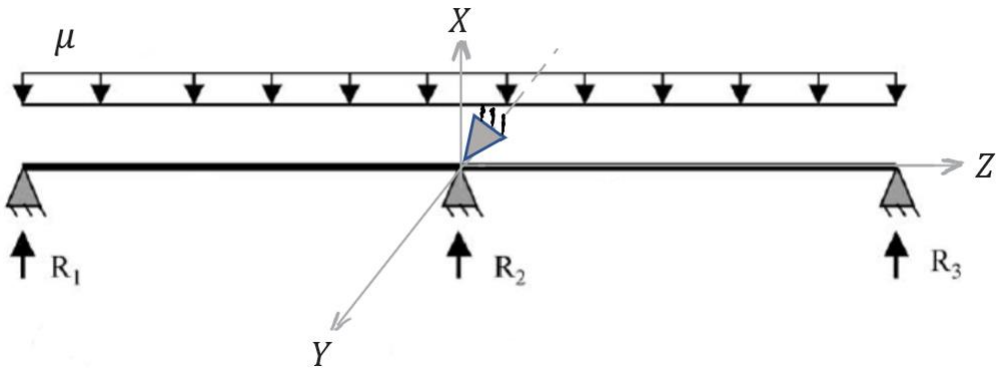

Figure 5.2 _ Two-span beam with one intermediate constraint

As it was discussed for one-span beam, procedure to assemble elements the elements of multi-span beam follow the same logic. After obtaining the global matrices and global nodal force vector, since all elements, displacements, and forces are expressed with respect to the same reference frame (global), the map matrix can be developed without considering the constraints at this stage.

$$\{q\} = \{u_{z1}\ u_{x1}\ u_{y1}\ \theta_{z1}\ \theta_{x1}\ \theta_{y1} \dots u_{z4}\ u_{x4}\ u_{y4}\ \theta_{z4}\ \theta_{x4}\ \theta_{y4}\}'_{1\times 24}$$

Table 5.2 _ Assembling table

	u_{z1} 1	u_{x1} 2	u_{y1} 3	θ_{z1} 4	θ_{x1} 5	θ_{y1} 6	u_{z2} 7	u_{x2} 8	u_{y2} 9	θ_{z2} 10	θ_{x2} 11	θ_{y2} 12	u_{z3} 13	u_{x3} 14	u_{y3} 15	θ_{z3} 16	θ_{x3} 17	θ_{y3} 18	…	θ_{x4} 23	θ_{y4} 24
1	u_{z1} 1	u_{x1} 2	u_{y1} 3	θ_{z1} 4	θ_{x1} 5	θ_{y1} 6	u_{z2} 7	u_{x2} 8	u_{y2} 9	θ_{z2} 10	θ_{x2} 11	θ_{y2} 12							…		
2							u_{z2} 1	u_{x2} 2	u_{y2} 3	θ_{z2} 3	θ_{x2} 4	θ_{y2} 5	u_{z3} 6	u_{x3} 7	u_{y3} 8	θ_{z3} 9	θ_{x3} 10	θ_{y3} 11	…		
3													u_{z3} 1	u_{x3} 2	u_{y3} 3	θ_{z3} 4	θ_{x3} 5	θ_{y3} 6	…	θ_{x4} 11	θ_{y4} 12

Once the mapping is done the global mass and stiffness matrices will be of the structure as what we have seen in single-span beam.

the global equation of motion of the entire structure with proportional damping is:

$$\boldsymbol{M}_T\ddot{\boldsymbol{q}} + \boldsymbol{C}_T\dot{\boldsymbol{q}} + \boldsymbol{K}_T\boldsymbol{q} = \boldsymbol{f}_T(t) \tag{5.6}$$

5.2 Boundary Conditions and Static equilibrium

Within a multi-span beam, the intermediate support, in our case, which is usually a pulley on which the cable passes, constraints only the vertical and lateral degrees of freedom (u_{Xi}, u_{Yi}) on the node i which is in the surface contact of the pulley. As a result, the pulley can simply be modeled by adding only two strong translational stiffness (k_i, χ_i) at the corresponding DOFs within the global stiffness matrix of the whole structure.

Considering the same small example, we discussed in section 4.1.3, but this time, the third node is constrained by the pulley, with a similar boundary condition at left and right end sides. Therefore, the displacement vectors of the constraint nodes would be as:

$$\{q_1\} = \begin{Bmatrix} u_{z1} \\ u_{X1} \\ u_{Y1} \\ \theta_{z1} \\ \theta_{X1} \\ \theta_{Y1} \end{Bmatrix} = \begin{Bmatrix} 0 \\ 0 \\ 0 \\ 0 \\ 0 \\ 0 \end{Bmatrix}, \quad \{q_3\} = \begin{Bmatrix} u_{z3} \\ u_{X3} \\ u_{Y3} \\ \theta_{z3} \\ \theta_{X3} \\ \theta_{Y3} \end{Bmatrix} = \begin{Bmatrix} u_{z3} \\ 0 \\ 0 \\ \theta_{z3} \\ \theta_{X3} \\ \theta_{Y3} \end{Bmatrix}, \quad \{q_4\} = \begin{Bmatrix} u_{z1} \\ u_{X1} \\ u_{Y1} \\ \theta_{z1} \\ \theta_{X1} \\ \theta_{Y1} \end{Bmatrix} = \begin{Bmatrix} u_{z1} \\ 0 \\ 0 \\ 0 \\ 0 \\ 0 \end{Bmatrix}$$

Adopting the same solution, k and χ are the relevant stiffnesses that are to be added to global stiffness matrix implementing respectively on translational and rotational DOFs. The additional stiffnesses are as the following:

$$\{k_{z1}\ k_{X1}\ k_{Y1}\ \chi_{z1}\ \chi_{X1}\ \chi_{Y1}\ k_{X3}\ k_{Y3}\ k_{X4}\ k_{Y4}\ \chi_{z4}\ \chi_{X4}\ \chi_{Y4}\}$$

Incrementation of potential energy due to additional stiffnesses is:

$$\Delta U = \frac{1}{2}k_{z1}(u_{z1})^2 + \frac{1}{2}k_{X1}(u_{X1})^2 + \frac{1}{2}k_{Y1}(u_{Y1})^2 + \frac{1}{2}\chi_{z1}(\theta_{z1})^2 + \frac{1}{2}\chi_{X1}(\theta_{X1})^2 + \frac{1}{2}\chi_{Y1}(\theta_{Y1})^2 + \cdots$$
$$\ldots + \tfrac{1}{2}k_{X3}(u_{X3})^2 + \tfrac{1}{2}k_{Y3}(u_{Y3})^2 + \tfrac{1}{2}k_{X4}(u_{X4})^2 + \tfrac{1}{2}k_{Y4}(u_{Y4})^2 + \tfrac{1}{2}\chi_{z4}(\theta_{z4})^2 + \tfrac{1}{2}\chi_{X4}(\theta_{X4})^2 +$$
$$\cdots + \tfrac{1}{2}\chi_{Y4}(\theta_{Y4})^2$$

$$\frac{d}{dt}\left(\frac{\partial \Delta U}{\partial u_{z1}}\right) = k_{z1}u_{z1}$$

$$\frac{d}{dt}\left(\frac{\partial \Delta U}{\partial u_{X1}}\right) = k_{X1}u_{X1}$$

$$\frac{d}{dt}\left(\frac{\partial \Delta U}{\partial u_{Y1}}\right) = k_{Y1}u_{Y1}$$

$$\frac{d}{dt}\left(\frac{\partial \Delta U}{\partial \theta_{z1}}\right) = \chi_{z1}\theta_{z1}$$

$$\frac{d}{dt}\left(\frac{\partial \Delta U}{\partial \theta_{X1}}\right) = \chi_{X1}\theta_{X1}$$

$$\frac{d}{dt}\left(\frac{\partial \Delta U}{\partial \theta_{y1}}\right) = \chi_{Y1}\theta_{Y1}$$

$$\frac{d}{dt}\left(\frac{\partial \Delta U}{\partial u_{X4}}\right) = k_{X4}u_{X4}$$

$$\frac{d}{dt}\left(\frac{\partial \Delta U}{\partial u_{Y4}}\right) = k_{Y4}u_{Y4}$$

$$\frac{d}{dt}\left(\frac{\partial \Delta U}{\partial \theta_{z4}}\right) = \chi_{z4}\theta_{z4}$$

$$\frac{d}{dt}\left(\frac{\partial \Delta U}{\partial \theta_{x4}}\right) = \chi_{x4}\theta_{x4}$$

$$\frac{d}{dt}\left(\frac{\partial \Delta U}{\partial \theta_{Y4}}\right) = \chi_{Y4}\theta_{Y4}$$

$$\frac{d}{dt}\left(\frac{\partial \Delta U}{\partial u_{X3}}\right) = k_{X3}u_{X3}$$

$$\frac{d}{dt}\left(\frac{\partial \Delta U}{\partial u_{Y3}}\right) = k_{Y3}u_{Y3}$$

$$\begin{bmatrix} \blacksquare + k_{z1} & \blacksquare & \blacksquare & \cdots & 0 & 0 & \cdots & 0 & 0 \\ \blacksquare & \blacksquare + k_{x1} & \blacksquare & \cdots & 0 & 0 & \cdots & 0 & 0 \\ \blacksquare & \blacksquare & \blacksquare + k_{y1} & \cdots & 0 & 0 & \cdots & 0 & 0 \\ \blacksquare & \blacksquare & \blacksquare & \ddots & \vdots & \vdots & \cdots & 0 & 0 \\ \blacksquare & \blacksquare & \blacksquare & \cdots & \blacksquare + \chi_{X3} & \blacksquare & \cdots & 0 & 0 \\ \blacksquare & \blacksquare & \blacksquare & \cdots & \blacksquare & \blacksquare + \chi_{Y3} & \cdots & 0 & 0 \\ \vdots & \vdots & \vdots & \vdots & \vdots & \vdots & \ddots & \vdots & \vdots \\ 0 & 0 & 0 & 0 & 0 & 0 & \cdots & \blacksquare + \chi_{X4} & \blacksquare \\ 0 & 0 & 0 & 0 & 0 & 0 & \cdots & \blacksquare & \blacksquare + \chi_{Y4} \end{bmatrix} \begin{Bmatrix} u_{z1} \\ u_{X1} \\ u_{Y1} \\ \vdots \\ u_{X3} \\ u_{Y3} \\ \vdots \\ \theta_{X24} \\ \theta_{Y24} \end{Bmatrix}$$

5.2.1 Calculation of Static equilibrium and Reaction Forces

The static displacement of the system due to the weight of the cable:

$$\boldsymbol{K_T q_S = f_T} \qquad \rightarrow \qquad \boldsymbol{q_S = K_T^{-1} f_T} \tag{5.7}$$

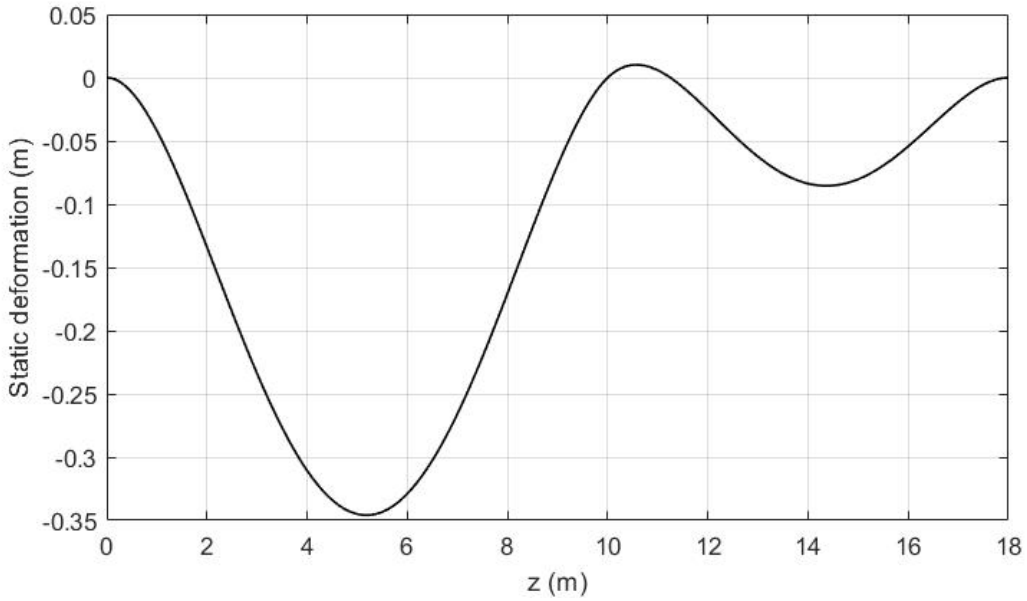

Figure 5.3 _ Static equilibrium

To calculate the reaction forces on pulley, we adopt the same logic used for boundary reaction forces

$$F_{z1} = k_{z1}u_{z1}$$
$$F_{X1} = k_{X1}u_{X1}$$
$$F_{Y1} = k_{Y1}u_{Y1}$$
$$M_{z1} = \chi_{z1}\theta_{z1}$$
$$M_{X1} = \chi_{X1}\theta_{X1}$$
$$M_{Y1} = \chi_{Y1}\theta_{Y1}$$
$$F_{X2} = k_{X2}u_{X2}$$
$$F_{Y2} = k_{Y2}u_{Y2}$$
$$M_{z2} = \chi_{z2}\theta_{z2}$$
$$M_{X2} = \chi_{X2}\theta_{X2}$$
$$M_{Y2} = \chi_{Y2}\theta_{Y2}$$
$$F_{X3} = k_{X3}u_{X3}$$
$$F_{Y3} = k_{Y3}u_{Y3}$$

5.3 Modal analysis of the system and validation

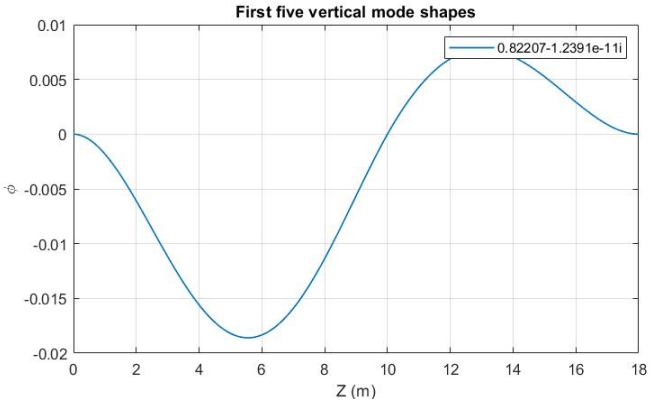

Figure 5.5 _ The 1st vertical mode

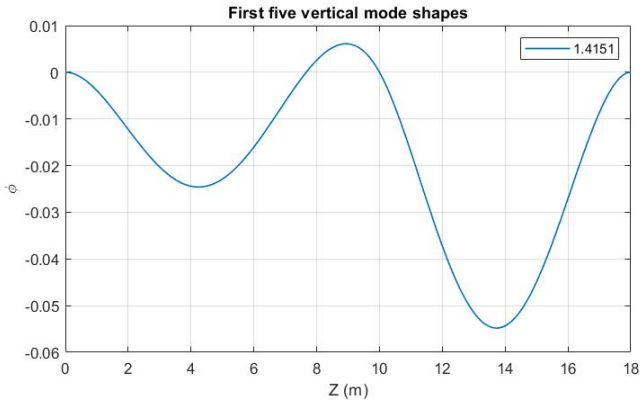

Figure 5.4 _ The 2nd vertical mode

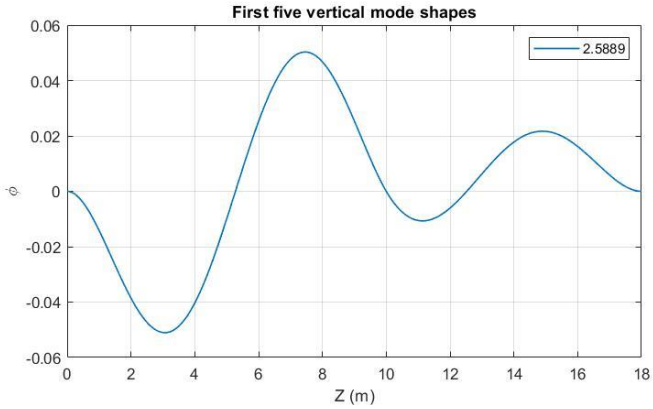

Figure 5.7 _ The 3rd vertical mode

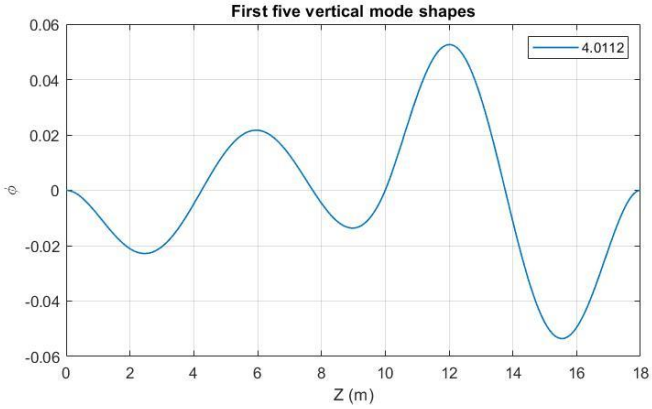

Figure 5.6 _ The 4th vertical mode

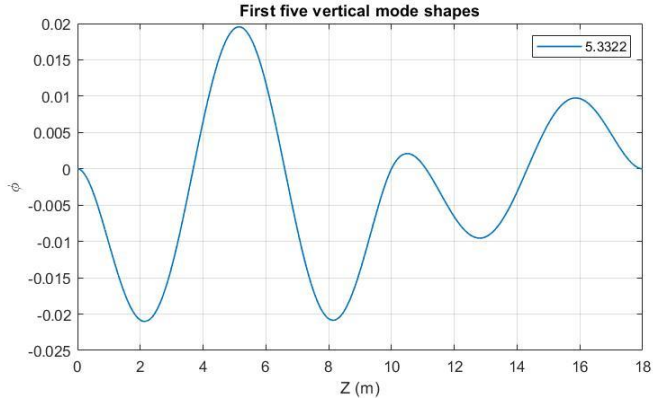

Figure 5.9 _ The 5th vertical mode

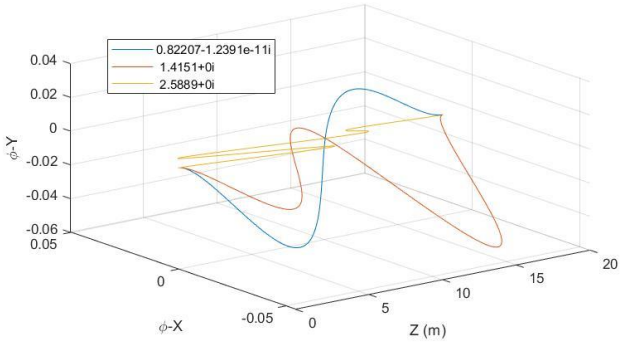

Figure 5.8 _ The first 3 modes in 3D space

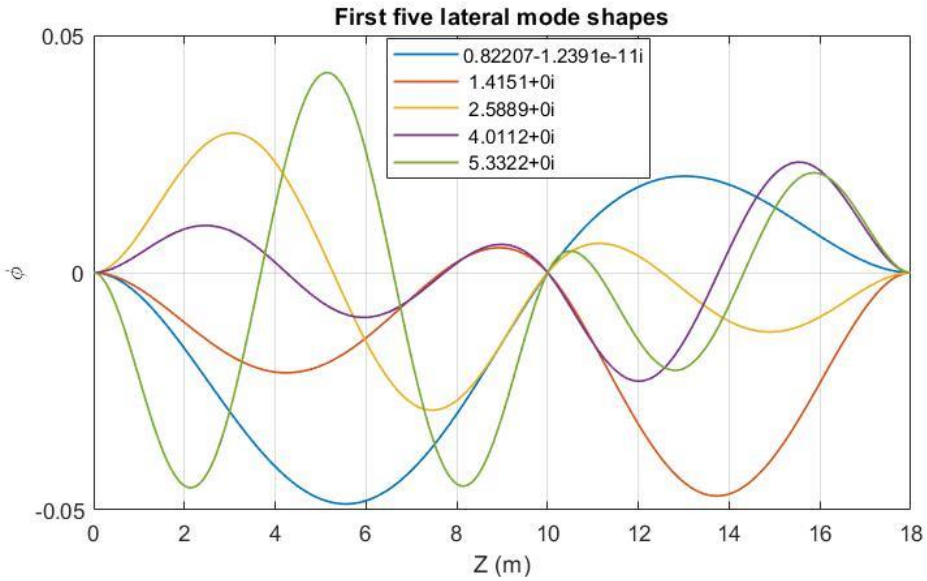

Figure 5.10 _ The first five modes in lateral direction

As we set the pretention T equal to zero, we would not have anymore stiffening effect caused by axial load, therefore we the range of frequencies are low. According to the different validation which have performed, these are promising and reliable.

Table 5.3 _ Natural frequency values (Hz)

Direction	First mode (Hz)	Second mode (Hz)	Third mode (Hz)	Forth mode (Hz)	Fifth mode (Hz)
Vertical – along X	0.82207	1.4151	2.5889	4.0112	5.3322
Lateral – along Y	0.82207	1.4151	2.5889	4.0112	5.3322

5.4 Dynamic responses of the system

To study the dynamic equation:

$$\boldsymbol{M}_T\ddot{\boldsymbol{q}} + \boldsymbol{C}_T\dot{\boldsymbol{q}} + \boldsymbol{K}_T\boldsymbol{q} = \boldsymbol{f}_T(t) \tag{5.8}$$

With proportional damping parameters α and β the same as previous case of study, respectively 0 and $\frac{1}{4}$, the same consideration about initial conditions $q_0, \dot{q}_0$, time step dt, and time integration scheme have been adopted:

$$\boldsymbol{q}_0 = \boldsymbol{q}_s \quad \& \quad \dot{\boldsymbol{q}}_0 = \{\boldsymbol{0}\} \quad \& \quad dt = 0.5e^{-3}s$$

5.4.1 Step Response

The same step function excites the system acting on a node located at $z = 7m$ starting at $t = 0$ and lasts for 2 seconds:

$$f(t) = \begin{cases} 0, & t < 0 \\ F_0, & 0 \le t \le 2 \\ 0, & t \ge 2 \end{cases} \quad \& \quad F_0 = -2\ kN$$

The nodal force vector of the node which is subjected to the load:

$$\boldsymbol{f}_n = \{0 \quad f(t) \quad 0 \quad 0 \quad 0 \quad 0\}$$

Results

In figure 5.11, time history of the displacement of two nodes (one node at each span) is depicted, and figure 5.12, displays the reaction forces due to step response of the system.

The natural frequencies are low, and since step response is kind of free response over new equilibrium, we can see the response takes place at a very low speed over time.

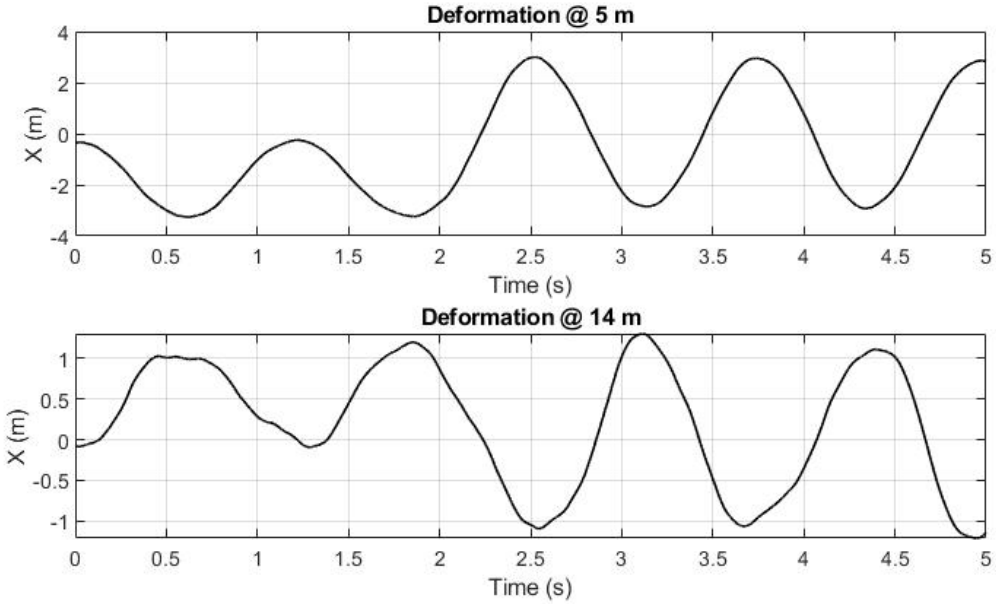

Figure 5.11_ Step response of two nodes at 5m & 14m

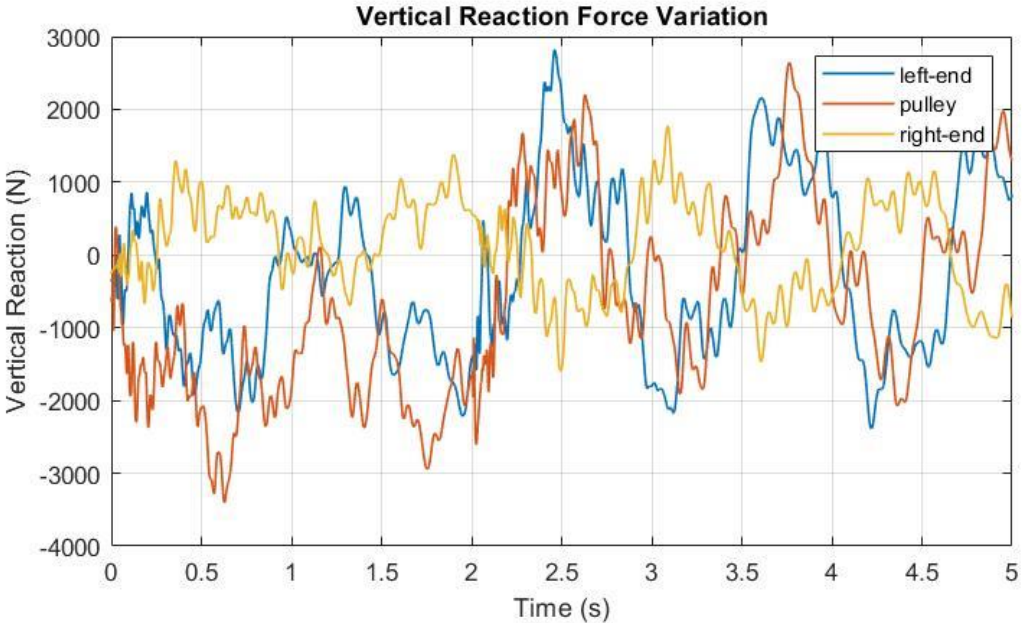

Figure 5.12 _ Variation of reaction forces over time

5.4.2 Harmonic Response

Here the aim is to study of the two-span beam response to a harmonic load with frequency $\varphi = 1\,Hz$ (close to first natural frequency).

$$f(t) = F_0 \sin(2\pi\varphi t)$$

The nodal force vector of the node on which the load acts:

$$\boldsymbol{f}_n = \{0 \quad f(t) \quad 0 \quad 0 \quad 0 \quad 0\}$$

The first natural frequency of the system is $\varphi_1 = 0.82207Hz$, and the frequency of the harmonic load is set close to it, $\varphi = 1\,Hz$. Since the exciting frequency is close to one of the natural frequencies beating kind of behavior can be detected. The load is applied on a node at $z = 4m$.

Result

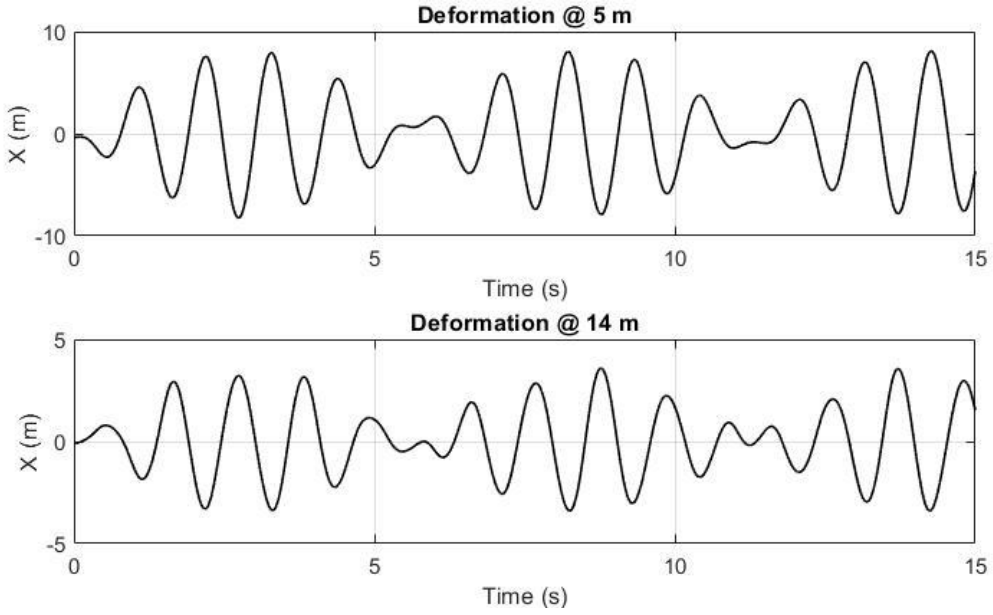

Figure 5.13 _ Harmonic response of two nodes at 5m & 14m

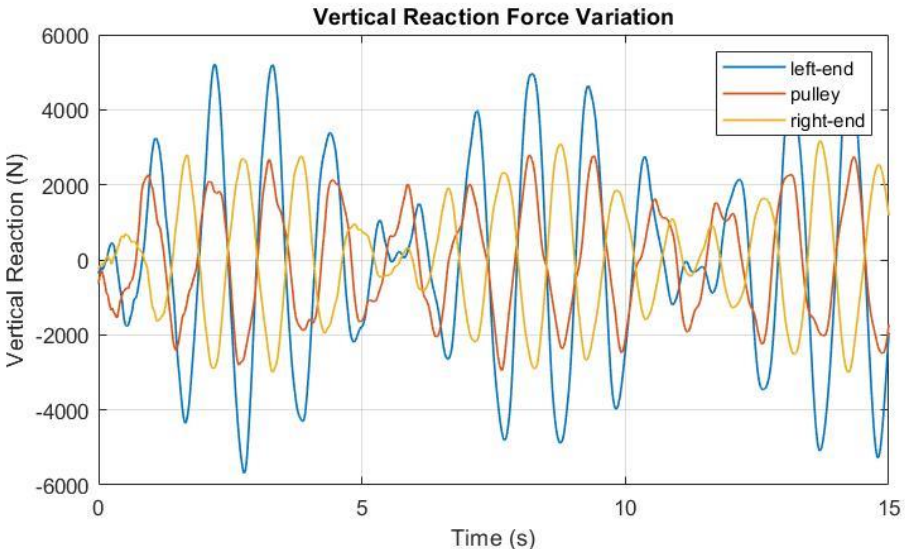

Figure 5.14 _ Variation of reaction forces over time

5.4.3 Response to moving load

6 3rd Configuration: Multi-Span beam carrying multiple lumped elements and a lumped system

To prove the accuracy and reliability of our simulation, we went with validation through a paper on "Journal of Sounds and Vibration".

This paper introduced a numerical assembly method (NAM) to find the correct values of natural frequencies and mode shapes of a multi-span Timoshenko beam. The mentioned beam carries multiple lumped elements and a seismic lumped system.

The configuration that we adopt to simulate and validate our work, is a pinned-pinned beam with an intermediate pin support which is depicted in figure 6.1.

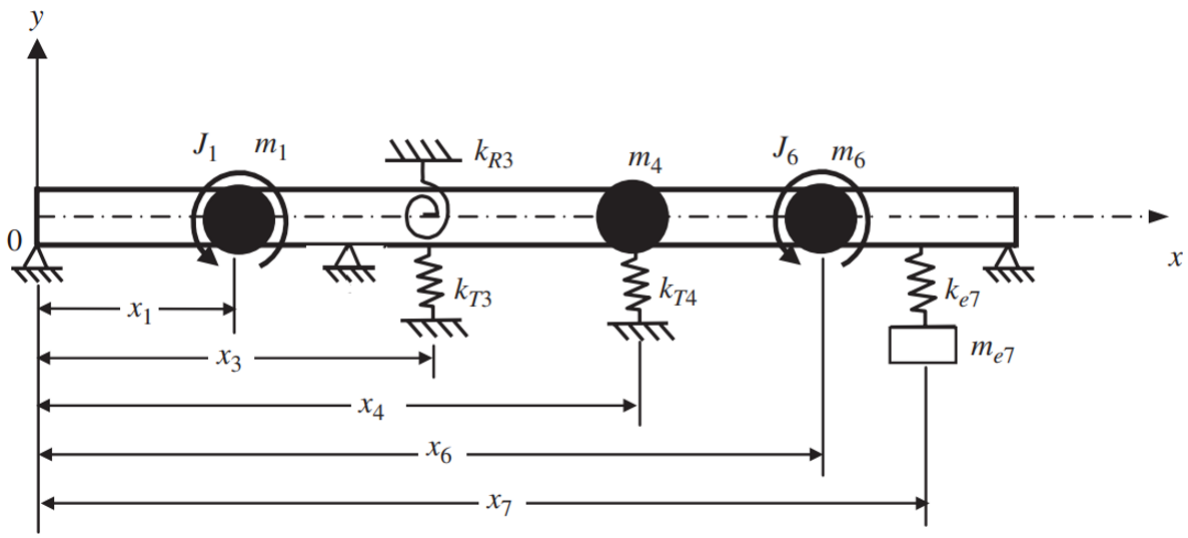

Figure 6.1 _ Sketch for a uniform Timoshenko beam supported by r intermediate pins, carrying u spring–mass systems and v various

Table 6.1 _ Geometric data and parameters of the system

Density ρ	$7.835e^3$ kg/m3	Rectangular cross section	
Elastic modulus E	$2.069e^{11}\ {}^{N}/_{m^2}$	Width b_I	0.05m
Shear coefficient k'	${}^{5}/_{6}$	Height h_I	0.06m
Poisson ratio v	0.3	length l	1 m
Shear modulus G	$7.9577e^{10}\ {}^{N}/_{m^2}$		

All the elements and there corresponding values are expressed in table 6.1:

Table 6.2 _ Elements' values

	m_1 (kg)	m_4 (kg)	m_6 (kg)	J_1 (kgm^2)	J_6 (kgm^2)	k_{T3} $\left(\frac{N}{m}\right)$	k_{T4} $\left(\frac{N}{m}\right)$	k_{R3} (Nm)	m_{e7} (kg)	k_{e7} $\left(\frac{N}{m}\right)$
vlaues	4.701	4.701	9.402	0.04701	0.14103	$1.86210e^6$	$2.79315e^6$	$9.3105e^5$	4.701	$5.5863e^5$
location	x_1	x_4	x_6	x_1	x_6	x_3	x_4	x_3	x_7	x_7

And $x_1 = 0.2m,\ x_3 = 0.4m,\ x_4 = 0.6m, x_6 = 0.8m, x_7 = 0.9m.$

6.1 Introducing lumped elements to the system

To introduce the elements, we adopt the same approach we used to introduce constraints, but this time since there are masses and inertias, since they are associated with the kinetic energy, their presence in the system lead to the increment in kinetic energy:

Incrementation of kinetic energy (ΔT) in correspondence of for example, lumped mass m_1 and lumped inertia J_1 is:

$$\Delta T_{m_1} = \frac{1}{2} m_1 \left(\dot{u}_{x_{x1}}\right)^2 + \frac{1}{2} m_1 \left(\dot{u}_{y_{x1}}\right)^2 + \frac{1}{2} m_1 \left(\dot{u}_{z_{x1}}\right)^2$$

$$\Delta T_{J_1} = \frac{1}{2} J_1 \left(\dot{\theta}_{x_{x1}}\right)^2 + \frac{1}{2} J_1 \left(\dot{\theta}_{y_{x1}}\right)^2 + \frac{1}{2} J_1 \left(\dot{\theta}_{z_{x1}}\right)^2$$

In which the indices x_1 below each DOF, indicates that degree of freedom is associated with node which located at $x = x_1$.

Then:

$$\frac{d}{dt}\left(\frac{\partial \Delta T_{m_1}}{\partial \dot{u}_{x_{x1}}}\right) = m_1 \dot{u}_{x_{x1}} \qquad \frac{d}{dt}\left(\frac{\partial \Delta T_{J_1}}{\partial \dot{\theta}_{x_{x1}}}\right) = J_1 \dot{\theta}_{x_{x1}}$$

$$\frac{d}{dt}\left(\frac{\partial \Delta T_{m_1}}{\partial \dot{u}_{y_{x1}}}\right) = m_1 \dot{u}_{y_{x1}} \qquad \frac{d}{dt}\left(\frac{\partial \Delta T_{J_1}}{\partial \dot{\theta}_{y_{x1}}}\right) = J_1 \dot{\theta}_{y_{x1}}$$

$$\frac{d}{dt}\left(\frac{\partial \Delta T_{m_1}}{\partial \dot{u}_{z_{x1}}}\right) = m_1 \dot{u}_{z_{x1}} \qquad \frac{d}{dt}\left(\frac{\partial \Delta T_{J_1}}{\partial \dot{\theta}_{z_{x1}}}\right) = J_1 \dot{\theta}_{z_{x1}}$$

Then, in the global mass matrix of the system, the value $m_1$will be added to any translational DOFs associated with node on which m_1 is added, and in the same way, the value J_1will be added to any rotational DOFs associated with node on which J_1 is added.

6.2 Introducing lumped system (dynamic shock absorber) to the system

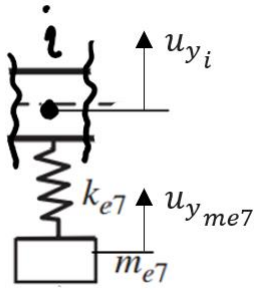

Figure 6.2 _ The seismic system attached to the beam at node i

As we can see from figure 6.2, the seismic system adds an additional degree of freedom ($u_{y_{me7}}$) to the node to which it is attached. In order to introduce the spring-mass system to the global mass and stiffness matrices, initially we add this DOF to global displacement vector, and by following similar procedure, the correspondence elements of matrices will be obtained:

$$\Delta T_{m_{e7}} = \frac{1}{2} m_{e7} \left(\dot{u}_{y_i} - \dot{u}_{y_{me7}} \right)^2$$

$$\Delta U_{k_{e7}} = \frac{1}{2} k_{e7} \left(u_{y_i} - u_{y_{me7}} \right)^2$$

$$\frac{d}{dt}\left(\frac{\partial \Delta T_{m_{e7}}}{\partial \dot{u}_{y_i}}\right) = m_{e7}\left(\dot{u}_{y_i} - \dot{u}_{y_{me7}}\right) \qquad \frac{d}{dt}\left(\frac{\partial \Delta U_{k_{e7}}}{\partial u_{y_i}}\right) = k_{e7}\left(u_{y_i} - u_{y_{me7}}\right)$$

$$\frac{d}{dt}\left(\frac{\partial \Delta T_{m_{e7}}}{\partial \dot{u}_{y_{me7}}}\right) = m_{e7}\left(-\dot{u}_{y_i} + \dot{u}_{y_{me7}}\right) \qquad \frac{d}{dt}\left(\frac{\partial \Delta U_{k_{e7}}}{\partial u_{y_{me7}}}\right) = k_{e7}\left(-u_{y_i} + u_{y_{me7}}\right)$$

Then the matrices will have additional elements as:

With respect to the stiffness matrix:

$$\begin{bmatrix} \ddots & \vdots & \vdots & \vdots & \iddots \\ \cdots & \blacksquare + k_{e7} & \cdots & 0 - k_{e7} & \cdots \\ \vdots & \vdots & \ddots & \vdots & \cdots \\ \cdots & 0 - k_{e7} & \cdots & 0 + k_{e7} & \cdots \\ \iddots & \vdots & \vdots & \vdots & \ddots \end{bmatrix} \begin{Bmatrix} \vdots \\ u_{y_i} \\ \vdots \\ u_{y_{me7}} \\ \vdots \end{Bmatrix}$$

With respect to the mass matrix:

$$\begin{bmatrix} \ddots & \vdots & \vdots & \vdots & \iddots \\ \cdots & \blacksquare + m_{e7} & \cdots & 0 - m_{e7} & \cdots \\ \vdots & \vdots & \ddots & \vdots & \cdots \\ \cdots & 0 - m_{e7} & \cdots & 0 + m_{e7} & \cdots \\ \iddots & \vdots & \vdots & \vdots & \ddots \end{bmatrix} \begin{Bmatrix} \vdots \\ u_{y_i} \\ \vdots \\ u_{y_{me7}} \\ \vdots \end{Bmatrix}$$

6.3 Results

The results have been compatible with those presented in the paper. In the following figure 6.3, depicts the first five modes from the paper for a Timoshenko beam, and figure 6.4, presents the corresponding results of our simulation:

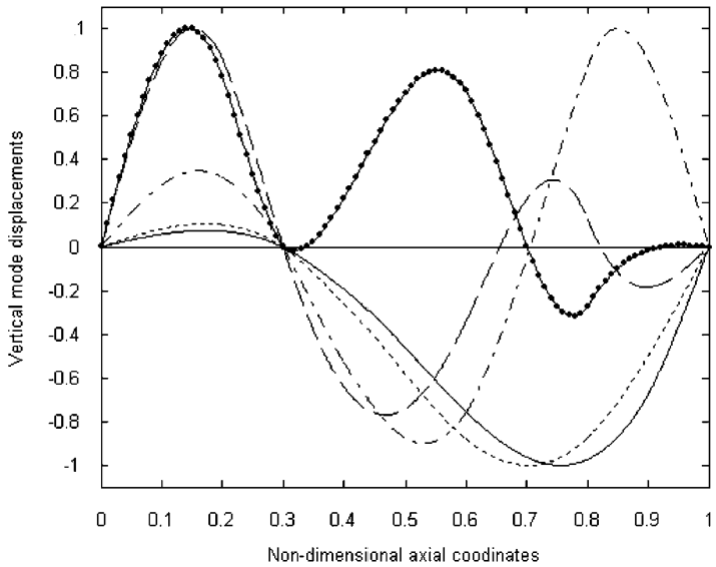

Figure 6.3 _ The lowest five mode shapes of the two-span pinned–pinned (P–P) Timoshenko beam carrying three point masses, two rotary

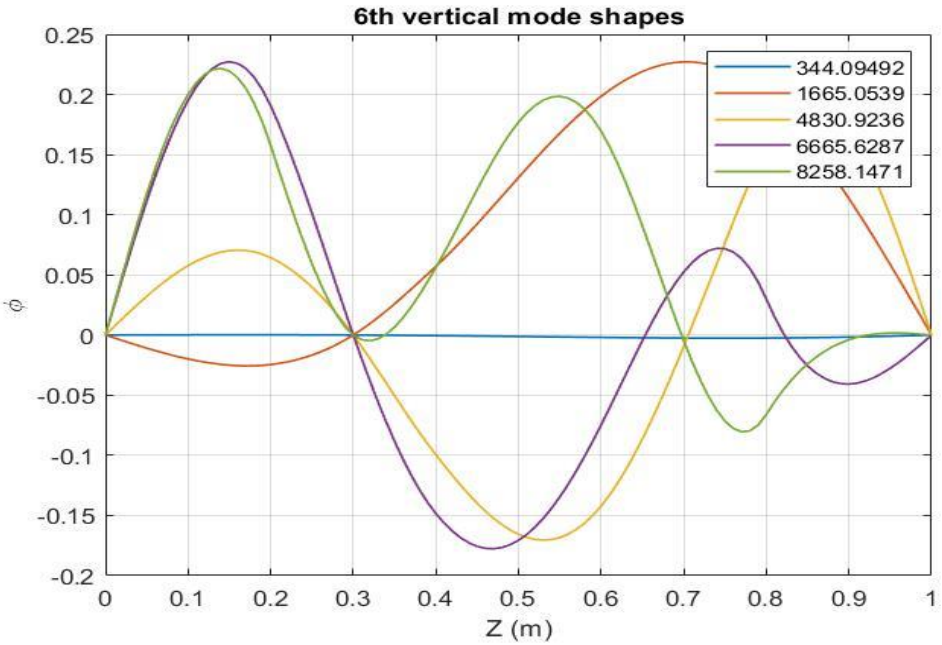

Figure 6.4 _ First five vertical mode shapes

Table 6.3 _ The lowest five natural frequencies of the two-span beam

Type of beam	Methods	ω_1 (rad/s)	ω_2 (rad/s)	ω_3 (rad/s)	ω_4 (rad/s)	ω_5 (rad/s)
Timoshenko beam	(NAM) paper	344.0505	1630.4214	4666.1223	6410.2455	7724.3333
Euler–Bernoulli beam	(NAM) paper	344.0948	1667.1936	4849.1637	6700.1525	8301.3915
Euler–Bernoulli beam	Present work	344.09492	1665.0539	4830.9236	6665.6287	8258.14171

7 Conclusion

8 Acknowledgement

9 List of figures

10 List of tables

11 Bibliography

Genta, G. (2008). Vibration dynamics and control . Springer.

M. Géradin, D. Rixen . (1997). Mechanical vibrations. John Wiley.

J. R. Rieker, Y.-H. Lin, and M. W. Trethewey. “Discretization considerations in moving load finite element beam models”. In: Finite elements in analysis and design 21.3 (1996), pp. 129–144.]!!!